

Experimental and theoretical study of corrosion inhibition effect of *Cucumeropsis mannii* N. seed oil metallic soap of zinc on mild steel surface in sulphuric acid

Ekemini B. Ituen^{*a}, Edidiong A. Essien^b, Uwemedimo E. Udo^a and Ogede R. Oluwaseyi^c

^aDepartment of Chemistry, Faculty of Science, University of Uyo, Akwa Ibom State, Nigeria

^bDepartment of Environmental Science, Cyprus International University, Turkey

^cDepartment of Science Technology, Federal Polytechnic, Ado-Ekitti, Ekitti State, Nigeria

ABSTRACT

*A new approach to characterizing the mechanism of adsorption of inhibitor molecules has been proposed from the findings of this study based on the degree of responsiveness of inhibition efficiency to changes in temperature. The adsorption and inhibition of mild steel corrosion in 1.0 M H₂SO₄ using different concentrations of zinc metallic soap of *Cucumeropsis mannii* N. was investigated at 303 - 333K via weight loss, hydrogen evolution and computational techniques using DFT at the B3LYP/6-31G* basis set level. Corrosion rate increased with increase in temperature both for the free acid and inhibited solutions, with marked reluctance to increase in corrosion rate for the inhibited solutions-reluctancy increasing with increase in concentration of the metallic soap of zinc. Inhibition efficiency increased with increase in the concentration of zinc soap. Addition of iodide ions further increased the inhibition efficiency indicating synergistic inhibition. The maximum inhibition efficiency of 70.1 % was obtained for 10 x 10⁻⁵ M zinc soap but increased to 85.3 % on addition of 0.001 M iodide ion. The adsorption was best described by the Langmuir adsorption isotherm from where negative values of Gibbs free energy change were obtained indicating spontaneity of the adsorption phenomena. Activation Energy was deduced from the Arrhenius equation while thermodynamic approach was used to elucidate the enthalpy and entropy of adsorption. Quantum chemical calculations reveal large energy gap between the LUMO and HOMO of the constituent fatty acids indicating a theoretically significant possibility of adsorption and mild steel-zinc soap molecules interactions. A new equation for temperature coefficient of inhibition efficiency (μ) was derived and applied for the first time using a classical physics concept and negative values of μ were obtained and interpreted as indicative of physical adsorption mechanism.*

Keywords: adsorption isotherm, *Cucumeropsis mannii* N., metallic soap inhibitors, mild steel, temperature coefficient of inhibition, zinc metallic soap.

INTRODUCTION

Metal corrosion is a major setback to optimum utility of metal-based structural materials globally. In industries where acids are used in pickling of iron and steel, chemical cleansing and processing, ore treatment and oil well acidification, acid corrosion has been a paramount problem as acids are known to be very corrosive. The acid H₂SO₄ tend to find extensive industrial application. Since acids are highly corrosive, the application of inhibitors serves to reduce the corrosive attack of the metals by the acids [1]. Corrosion of metals generally occur by processes relating to the protective surface oxide, which dissolves substantially when the metal is exposed to high concentration of acids or bases [2]. Once the oxide film becomes broken-down, the base metal surface becomes exposed to the aqueous corroding medium, which subsequently leads to a sequence of electro-chemical reactions. Such processes at

the base metal surface are uniquely dependent on the environment and usually result in insoluble complex that increases the rate of metal dissolution [3].

Like most chemical reactions, the rate of corrosion increases with increase in temperature. Therefore, industries operating processes at elevated temperatures are most vulnerable to experiencing great loss of their metallic components to corrosion. Usually, acid corrosion rate of metals increases gradually as temperature rises from room temperature to about 303K, while a sharp increase results when the temperature is increased to 313K. At higher temperatures up to 323K and above, the rate of metal corrosion becomes very high and the need for corrosion inhibitors becomes critical. Corrosion inhibition usually involves the addition of a substance or substances into any corroding environment with the intention of decreasing the corrosion rate of the metal. Therefore, a corrosion inhibitor may loosely be regarded as that substance which when added intentionally to an aggressive medium, decreases its rate of attack on a metal. Inhibitors are generally used to protect materials from deterioration due to corrosion [4]. Most of the well-known inhibitors used in industries are organic compounds having multiple bonds or containing nitrogen, sulphur, oxygen or phosphorus through which they get adsorbed onto the metal surface by means of their non-bonding electrons [5].

Inhibitors function by adherence to the metal surface thereby retarding metal dissolution by means of adsorption. This results in the formation of adsorbed film, which acts as a barrier, isolating the metal from the corrodent [6]. The nature of inhibitor adsorption and the degree of inhibition depends on the number and type of adsorption sites on the metal surface as well as the type of interaction between the organic molecule and the metal surface [7]. Corrosion inhibitors are commonly added to coolants, paints, fuels, hydraulic fluids, water boiler, engine oils, and many other fluids used in the industry. The efficiency of organic inhibitors in acid media has been reported to synergistically increase on addition of halide salts to the solution [8-10]. Several studies have been carried out using organic, inorganic and organometallic compounds, both natural and synthetic. Recent trends involve the use of either crude characterized extracts of plants stem, leaves, seeds or roots. The aim is basically to ensure that the inhibitor is efficient, cheap, readily available, stable and green. Most inhibitors are usually invented but scarcely incorporated into a system where their functionality could be ascertained. However, there seems to be no report available in literature on the use of metallic soaps as inhibitors of metal corrosion. The authors are therefore motivated by this fact to investigate and we report for the first time the application of metallic soap of zinc as corrosion inhibitor of mild steel. Experimental findings have also been backed up from theoretically calculated parameters using DFT at the B3LYP/6-31G*basis set level.

Metallic soaps are a group of compounds in which the acid hydrogen or the cation in a long chain monobasic acid has been replaced by a metal of the alkaline earth or heavy metals series [11]. They have the general formula $(RCOO)_yM$, where R is an aliphatic or alicyclic group, and M is a metal with valence $y : 1 \leq y \leq 2$. Their insolubility in water at low temperatures differentiates them from ordinary soaps of sodium and potassium while their solubility in organic solvents on the other hand, accounts for their application in a wide range of industrial products [12-13]. Metal soaps are used for different purposes, depending on the type: calcium or aluminium soaps are employed as water repellants in water proofing, textiles and walls [13]; zinc and magnesium stearates are used in large quantities by cosmetic industries to increase the smoothness, adhesion and water repellency of face and baby powders [12]; linoleates and linolenates of some transition metals salts are utilized as driers in printing inks and paints industries [14]; etc. Metallic soaps have also been used as plasticizers and driers in rubber-based adhesives [15].

The paint industry is probably the largest users of the highest volume of metallic soaps. With the phasing out of lead as the primary drier in paints, metallic soaps have become outstandingly essential a component in the manufacture of both emulsion and gloss paints. Soaps of the transition metals act as driers in paint, while those of aluminum, calcium and magnesium function as flattening or leveling agents [16]. Metallic soaps are available commercially and are offered as solids, liquids or powders. They are prepared from fatty acids either by fusion or precipitation processes. The use of paints for metal corrosion control spans over several centuries, especially gloss paint. Metallic soaps, recently, constitute components of these paints and they have contributed reasonably to improving the quality and acceptability of paints as reported by Essien *et al* [11]. This work is also aimed at determining the inhibition effect of one of the components of paints as well as making recommendations on the efficiency of such component-the metal soap. The choice of zinc soap made from melon (*Cucumeropsis mannii* Naud.) seed oil as inhibitor of mild steel corrosion is informed by its fatty acid composition namely Palmitic (10.57 %), Stearic (8.33 %), Oleic (13.65 %), Linoleic (62.14 %) and Linolenic (5.29 %) acids [11]. Oxygen atoms is present in their molecular structures and in addition, linoleic and linolenic acids contain double bonds, which constitute potential adsorption sites onto the mild steel surface by the donation of electrons to the empty d-orbital of Iron.

MATERIALS AND METHODS

2.1 Preparation of specimens mild steel

Mild steel sheet (thickness = 0.46mm) used in the study were supplied by Sky Aluminium Limited, Uyo, Nigeria, with composition (wt.%): 0.13 C, 0.18 Si, 0.39 Mn, 0.60 P, 0.04 S, 0.025 Cu, and bal Fe), were mechanically cut into 4.0 cm × 4.0 cm × 0.046 cm dimensions, washed in absolute ethanol and acetone, dried in room temperature and stored in a moisture free desiccator before their use in corrosion studies without further polishing [17].

2.2 Reagents

The corrodent was analytical grade (BDH) H₂SO₄ and the concentration prepared and used was 1.0 M. The inhibitor (metallic soap of Zinc) was synthesized and characterized according to Essien *et al.*, 2011 [11]. Different concentrations of the Zn soap used as inhibitor solution were prepared by dissolving respectively appropriate masses of accurately weighed sample of the inhibitor in about 5 cm³ of methanol, vigorously stirred until complete dissolution, quantitatively prepared in 1.0 M sulphuric acid solution. The concentration of KI used was 0.001M and was prepared from sample supplied by BDH, England.

2.3 Weight loss method

The weight loss measurement was conducted under total immersion of the pre-weighed mild steel coupons in 250 mL capacity beakers containing about 30 mL of the test solution. The coupons were retrieved at 2 hours interval progressively for 10 hours, washed thoroughly in 20% NaOH solution containing 200 g/L of zinc dust (ASTM G1-72, 1990) with thistle rush, rinsed convincingly in distilled water, cleaned, dried in acetone, and re-weighed using a FA2104A digital weighing balance with sensitivity ± 0.0001g. The differences in the weights of the mild steel coupons *ab initio* and after immersion in different test solutions were recorded as the weight loss. This was repeated for the different temperatures 303 - 333 K. To ensure reproducibility, experiments were carried out in triplicates and the standard deviation values among parallel triplicate experiments were found to be smaller than 3%, indicating reliability and reproducibility, and the mean values of the weight loss data were used for further computations. The corrosion rate was calculated from the weight loss data using the relationship:

$$CR = \Delta w/AT \quad (1)$$

where CR (mgcm⁻²h⁻¹) is the corrosion rate, Δw (g) is the weight loss of the mild steel in the test solutions, A (cm²) is the surface area of the coupons and T (s) is the total immersion time. The inhibition efficiency, I (%), was then computed using the equation:

$$\% I_w = 100 (CR_b - CR_i) / CR_b \quad (2)$$

Where CR_b and CR_i are the corrosion rates in the absence and presence of the inhibitor respectively and $\% I_w$ is the percentage inhibition efficiency using weight loss method. The degree of surface coverage, Θ , of the active sites of the inhibitor molecules on the metal surface was also computed using the relationship:

$$\Theta = I (\%) / 100 \quad (3)$$

2.4 Gasometric Method

Hydrogen evolution measurement was performed using gasometric assembly. Detailed description of the assembly has been reported elsewhere [18]. The procedure followed was similar to that reported by other author [19]. The progress of corrosion in the absence and presence of test inhibitor was monitored by careful measurement of the volume of hydrogen gas evolved at fixed time intervals. The experiment was performed for 1.0 M H₂SO₄ (blank) and for the solutions containing different concentrations of the Zn-soap at 303 – 333 K maintained using a thermostated water bath. Hydrogen evolution rate (RV_H) which can be correlated to the mild steel corrosion rate was computed based on the volume of hydrogen gas evolved using the expression:

$$RV_H = (V_1 - V_0) / (T_1 - T_0) \quad (4)$$

where V_1 and V_0 are volumes of hydrogen evolved at time T_1 and T_0 respectively. The inhibition efficiency ($\% I_H$) was computed using the equation:

$$\% I_H = 100(RV_{H(blank)} - RV_{H(inhib)}) / RV_{H(blank)} \quad (5)$$

where $RV_{H(blank)}$ and $RV_{H(inhib)}$ are the rate of hydrogen evolution in the absence and presence of the Zn-soap respectively.

2.5 Quantum Chemical Computation

Density Functional Theory (DFT) at the B3LYP/6-31G* basis set level using Spartan '10 wave function package was used to carry out quantum chemical calculations. Full geometry optimization, electronic excitation and vibrational analyses of the optimized structures for the fatty acid composition of the metallic soap of zinc (viz palmitic, linolenic, linoleic, stearic and oleic acid as neutral molecules. Relevant parameters were calculated theoretically which will be used to describe the inhibitor-metal interactions.

RESULTS AND DISCUSSION

3.1 Weight loss experiment

Weight loss data determined at the end of 10 hours time interval in the absence and presence of different concentrations of the Zn-soap were used to calculate the corrosion rates and the values of inhibition efficiencies and degree of surface coverage for the inhibition of mild steel corrosion in 1.0 M H_2SO_4 at 303 - 333 K as provided by equations 1 - 3. The corrosion rate decreased with increasing inhibitor concentration but increased with increase in temperature. Table 1 shows the corrosion rates and inhibition efficiencies under the stated conditions. An inhibition efficiency of 71.0 % and 57.7 % were obtained for the highest concentration of the Zn-soap (10 mg/L) at 303 and 333K respectively. This may be ascribed to the adsorption of the Zn-soap onto the mild steel surface at the metal-acid interface. The high inhibitive performance of Zn-soap even at high temperatures suggests a higher bonding ability of the inhibitor to the mild steel surface probably due to the large molecular structures of the fatty acids that constitute the Zn-soap and enhanced solubility at increased temperature. The addition of 0.001 M KI further increased the % *I* to 85.3 and 75.7 for the highest concentration of the inhibitor at 303 and 333 K respectively, indicating synergistic inhibition by the halide ions. The inhibition efficiencies obtained for weight loss and hydrogen evolution methods were comparable hence only values for weight loss has been used for calculations.

Table 1 (a): Corrosion rates and Inhibition efficiencies for the inhibition of mild steel corrosion in 1.0 M H_2SO_4 in the absence and presence of different concentrations of Zinc soap alone at 303 - 333 K using weight loss technique

| Inhibitor conc. (mg/L) | Corrosion rate (CR) ($mgcm^{-2}h^{-1}$) | | | | Inhibition Efficiency (% <i>I</i>) | | | |
|---------------------------|---|-------|--------|--------|-------------------------------------|-------|-------|-------|
| | 303 K | 313 K | 323 K | 333 K | 303 K | 313 K | 323 K | 333 K |
| 2 | 0.717 | 2.154 | 7.210 | 11.891 | 59.7 | 55.4 | 53.6 | 49.4 |
| 4 | 0.674 | 1.990 | 6.915 | 11.703 | 62.1 | 58.8 | 55.5 | 50.2 |
| 6 | 0.619 | 1.922 | 6.698 | 11.139 | 65.2 | 60.2 | 56.9 | 52.6 |
| 8 | 0.579 | 1.734 | 6.630 | 10.551 | 67.5 | 64.1 | 59.4 | 55.1 |
| 10 | 0.532 | 1.565 | 5.920 | 9.940 | 70.1 | 67.6 | 61.9 | 57.7 |
| Blank | 1.780 | 4.830 | 15.540 | 23.500 | - | - | - | - |

Table 1 (b): Corrosion rates and Inhibition efficiencies for the inhibition of mild steel corrosion in 1.0 M H_2SO_4 in the absence and presence of different concentrations of Zinc soap blended with 0.001 M KI at 303 -333 K using weight loss technique

| Inhibitor conc. (mg/L) | Corrosion rate (CR) ($mgcm^{-2}h^{-1}$) | | | | Inhibition Efficiency (% <i>I</i>) | | | |
|---------------------------|---|-------|--------|--------|-------------------------------------|-------|-------|-------|
| | 303 K | 313 K | 323 K | 333 K | 303 K | 313 K | 323 K | 333 K |
| 2 | 0.501 | 1.478 | 5.563 | 9.330 | 71.8 | 69.4 | 64.2 | 60.3 |
| 4 | 0.438 | 1.323 | 4.910 | 8.296 | 75.4 | 72.6 | 68.4 | 64.7 |
| 6 | 0.361 | 1.140 | 4.226 | 7.449 | 79.7 | 76.4 | 72.8 | 68.3 |
| 8 | 0.301 | 0.966 | 3.636 | 6.392 | 83.1 | 80.0 | 76.6 | 72.8 |
| 10 | 0.262 | 0.845 | 3.201 | 5.711 | 85.3 | 82.5 | 79.4 | 75.7 |
| Blank | 1.780 | 4.830 | 15.540 | 23.500 | - | - | - | - |

Table 1 (c): Corrosion rates and Inhibition efficiencies for the inhibition of mild steel corrosion in 1.0 M H_2SO_4 in the absence and presence of different concentrations of Zinc soap alone at 303 -333 K using hydrogen evolution technique

| Inhibitor conc. (mg/L) | Corrosion rate (CR) ($mgcm^{-2}h^{-1}$) | | | | Inhibition Efficiency (% <i>I</i>) | | | |
|---------------------------|---|-------|-------|-------|-------------------------------------|-------|-------|-------|
| | 303 K | 313 K | 323 K | 333 K | 303 K | 313 K | 323 K | 333 K |
| 2 | 0.239 | 0.348 | 0.688 | 1.312 | 58.7 | 56.0 | 54.1 | 50.5 |
| 4 | 0.211 | 0.320 | 0.659 | 1.288 | 63.6 | 59.5 | 56.1 | 51.4 |
| 6 | 0.197 | 0.297 | 0.637 | 1.240 | 66.1 | 62.4 | 57.5 | 53.2 |
| 8 | 0.190 | 0.279 | 0.618 | 1.192 | 67.2 | 64.6 | 58.8 | 55.0 |
| 10 | 0.171 | 0.251 | 0.568 | 1.129 | 70.5 | 68.2 | 62.1 | 57.4 |
| Blank | 0.580 | 0.790 | 1.500 | 2.650 | - | - | - | - |

Table 1 (d): Corrosion rates and Inhibition efficiencies for the inhibition of mild steel corrosion in 1.0 M H₂SO₄ in the absence and presence of different concentrations of Zinc soap blended with 0.001M KI at 303 -333 K using hydrogen evolution technique

| Inhibitor conc. (mg/L) | Corrosion rate (CR) (mgcm ⁻² h ⁻¹) | | | | Inhibition Efficiency (% I) | | | |
|---------------------------|---|-------|-------|-------|-----------------------------|-------|-------|-------|
| | 303 K | 313 K | 323 K | 333 K | 303 K | 313 K | 323 K | 333 K |
| 2 | 0.169 | 0.245 | 0.549 | 1.073 | 70.9 | 69.0 | 63.4 | 59.5 |
| 4 | 0.144 | 0.219 | 0.463 | 0.927 | 72.3 | 71.3 | 69.1 | 65.0 |
| 6 | 0.124 | 0.188 | 0.412 | 0.848 | 78.7 | 76.2 | 72.5 | 68.0 |
| 8 | 0.099 | 0.162 | 0.358 | 0.745 | 82.9 | 79.5 | 76.1 | 71.9 |
| 10 | 0.081 | 0.141 | 0.303 | 0.657 | 86.0 | 82.2 | 79.8 | 75.2 |
| Blank | 0.580 | 0.790 | 1.500 | 2.650 | - | - | - | - |

3.2 Adsorption Considerations

Several mechanisms have been proposed as descriptive of the adsorption of organic molecules onto a metal surface. The mechanism of adsorption of Zn soap onto the mild steel surface would be similar that reported by [20]. If a molecule/ion M⁻ is adsorbed on the steel surface, a surface complex ion forms in the anodic process, and the complex is then desorbed from the surface according to the equations:



where 's' represents a species (ion or compound) at the surface. Obviously, the degree of inhibition of the metal corrosion or retardation of its dissolution in the aggressive medium will be dependent on the stability of the ion or complex formed at the surface. The inhibitor molecule functions by blocking the active sites on the surface of the metal, thereby reducing the corrosion rate. Increase in concentration of the Zn-soap increases the amount of the surface complex formed, resulting in greater inhibition of the corrosion process. In order to ascertain and quantitatively describe certain parameters associated with the adsorption behavior of the zinc soap, the surface coverage data obtained from the corrosion rate in the presence, CR_i , and absence, CR_b , of the inhibitor in the acid solution, were fitted into adsorption isotherms and the model that best fits the adsorption process was used to describe the adsorption process from the R² values of the linear plots. The models attempted were Frumkin, Temkin, Langmuir, Freundlich, Florry-Huggins and El-Awady *et al* adsorption models. These models, in their respective ways, are described by the equation

$$f(\theta, x) \exp(-2a\theta) = kC \quad (11)$$

where $f(\theta, x)$ represents the configuration factor and depends on the physical model and the assumptions underlying the derivation of the model, θ is the degree of surface coverage, C is the concentration of the inhibitor in the aggressive medium, x is the size ratio, 'a' is the molecular interaction parameter and k is the equilibrium constant of the adsorption process. The adsorption of Zn soap was by far best described by Langmuir model which is associated with description of the ideal physical and chemical adsorption process, and where no interaction exists between the adsorbate and the adsorbent. According to the model,

$$C/\theta = 1/K_{ads} + C \quad (12)$$

Linear plots of C/θ against C for Zn-soap alone and Zn-soap blended with 0.001M KI for weight loss measurement should yield an intercept of $1/k$ and as depicted in figure 1 below.

Ideally, these plots should yield unit slopes. The linearity of the plots above may be taken to mean that Zn-soap adsorption obeys the Langmuir model, but the considerable deviation of the slopes from unity shows that the isotherm cannot be strictly applied in the description of adsorption parameters. This deviation from unity is attributed to interactions between adsorbate species on the metal surface as well as changes in the adsorption heat with increasing surface coverage [11]. Therefore, a modified Langmuir equation suggested elsewhere [21] given in equation (13) below that takes care of this deviation may be used:

$$C/\theta = n/K_{ads} + nC \quad (13)$$

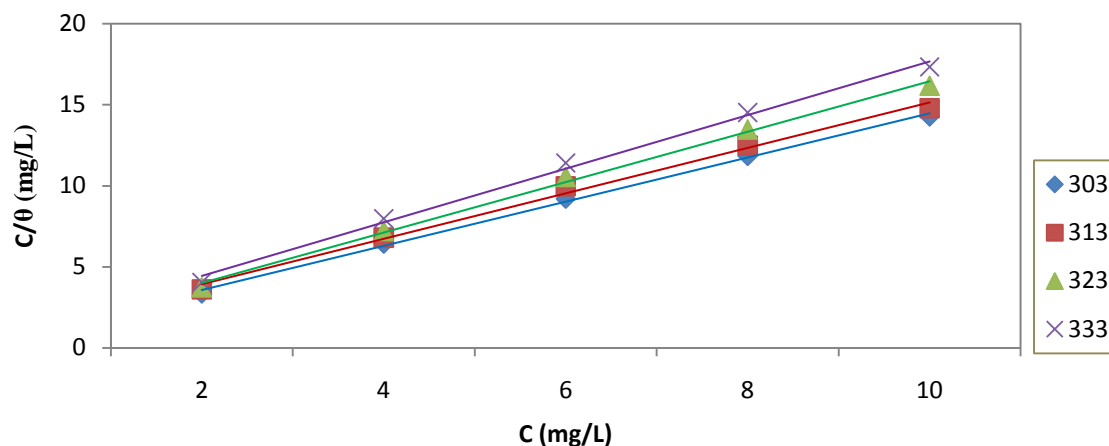


Fig. 1 (a): Langmuir adsorption isotherm for the inhibition of mild steel corrosion in 1.0 M H₂SO₄ in the presence of different concentrations of metallic Zn-soap at 303 -333 K

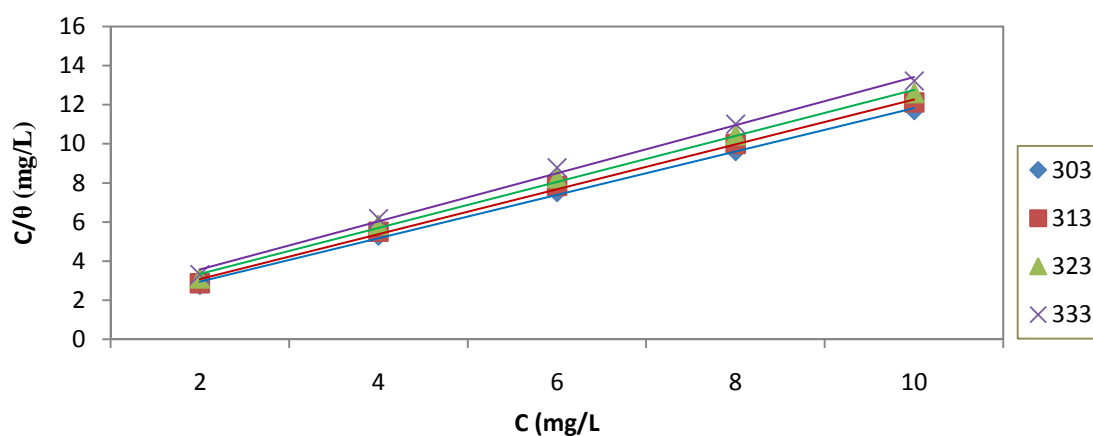


Fig 1 (b): Langmuir adsorption isotherm for the inhibition of mild steel corrosion in 1.0 M H₂SO₄ in the presence and absence of different concentrations of metallic Zn-soap blended with 0.001 M KI at 303 -333 K

The relationship between K_{ads} and free energy of adsorption (ΔG^*_{ads}) is given by

$$K = 0.018 \exp (-\Delta G^*_{ads}/RT) \tag{14}$$

where 0.018 is the reciprocal of 55.5 which represents the concentration of water and T is the operating temperature.

Table 2 shows the adsorption parameters deduced from the Langmuir isotherm.

Table 2: Langmuir adsorption parameters for Zn soap and Zn soap in 0.001M KI at different temperatures

| Temp (K) | K_{ads} | $-\Delta G_{ads}(\text{kJmol}^{-1})$ |
|---------------------|-----------|--------------------------------------|
| 303 | 3.217 | 43.10 |
| 313 | 2.508 | 41.03 |
| 323 | 3.512 | 43.83 |
| 333 | 2.948 | 42.37 |
| Zn soap + 0.001M KI | | |
| 303 | 2.989 | 42.49 |
| 313 | 2.941 | 42.35 |
| 323 | 2.379 | 40.59 |
| 333 | 2.200 | 39.94 |

Adsorption of organic molecules onto metal surfaces may occur by electrostatic interaction between charged molecules and the charged metal surface; it may also occur by interaction of unshared electron pairs in the molecule and the metal or by interaction of π -electrons of the molecules with the metal, or both. In any case, the strength of interaction between the adsorbate and the adsorbent is often revealed in the values of the adsorption-desorption equilibrium constant, K_{ads} . The large K_{ads} values obtained denote efficient adsorption and thus better inhibition efficiency, while the positive values obtained may be ascribed to appreciable strengths of Zn soap – mild steel

interaction as a function of temperature. The computed free energy of adsorption values, ΔG_{ads}^{θ} , were negative, indicating spontaneous nature of adsorption of the Zn soap onto the metal surface, and the values agree with physical adsorption mechanism arising from interaction between π -electrons of inhibitor molecules with the d-orbital electrons of the metal [22].

3.3 Quantum Chemical Computation Details

Density functional theory (DFT) is a useful tool for probing the interaction between an inhibitor and the metal surface and also for analyzing the experimental data. Therefore it was employed in order to explain experimental results obtained and further gain insight into the inhibitory action and mechanism of the zinc metallic soap at the acid-mild steel interface. The optimized geometry of the constituents of fatty acids are shown in figure 2. Figures 3 and 4 show the highest occupied molecular orbital (HOMO) density and lowest unoccupied molecular orbital (LUMO) density respectively of the fatty acid constituents of the metallic soap using DFT at the B3LYP/6-31G* basis set level. The density of the fatty acid constituents is shown in figure 5. Tables 3, 4 and also show some molecular properties, Mullikan charge distribution and bond order respectively of the fatty acid constituents calculated using DFT at the B3LYP/6-31G* basis set level. Using the same set, the orbital energies of the fatty acids are shown in figure 6 while the infrared spectra of the fatty acids are shown in figure 7.

The reactivity of a given inhibitor molecule has been associated with its molecular orbital, namely, HOMO and LUMO. The higher the HOMO energy (E_{HOMO}) for a given molecule, the higher the ability of the molecule to donate electrons to an appropriate acceptor having low-energy empty molecular orbital, hence the adsorption on the metal surface by means of π electrons. E_{LUMO} is associated with electron accepting tendency of a molecule. The energy difference or band-gap, ($\Delta E = E_{LUMO} - E_{HOMO}$), calculated is shown in Table 3. It can be seen that palmitic acid (% composition = 10.57) and stearic acid (% composition = 8.33) possess the highest difference in orbital energy (ΔE) with a value of 7.76 eV followed by oleic acid [(% composition = 13.65), (6.67 eV)], linolenic acid [(% composition = 13.65), (6.64 eV)] and linoleic acid [(% composition = 62.14), (6.63 eV)]. The HOMO and LUMO density were mainly concentrated on the oxygen atoms, double bonds and the carbonyl functional groups. It is therefore expected that the vacant orbitals of the iron will accept electrons from these groups on the inhibitor constituents. Also, the band-gap values obtained [being reasonably low] may be associated with high chemical reactivity, high polarizability, low kinetic stability and softness of the fatty acid molecules [27]. The infra-red spectra of the constituents reveal possible major absorptions at wavelengths corresponding to carbonyl group, aliphatic -OH group and C=C bonds, which suggests that these functional groups constitute the adsorption sites of the inhibitor onto the metal surface.

The dipole moment of each of the fatty acid phytochemicals were also calculated. Dipole moment is usually associated with non-uniform distribution of charges on the various atoms in a molecule which makes it useful for studying intermolecular interactions such as van der Waals type, dipole-dipole forces, etc [27]. The obtained values are in the range 1.24 - 1.78 debye ($4.13 - 5.93 \times 10^{-30}$ Cm) and are less than that of water (6.23×10^{-30} Cm) which supports the weakness in the force of attraction and hence the physical adsorption mechanism earlier proposed.

3.4 Temperature Coefficient of Inhibition Efficiency

A new approach to characterizing the mechanism of adsorption of inhibitors is being proposed i.e. from temperature coefficient of inhibition efficiency. Temperature coefficient of inhibition efficiency is quantitatively defined here as the degree of responsiveness of inhibition efficiency to changes in temperature. A linear relationship is assumed to exist between temperature change and the change in inhibition efficiency for a given concentration of the inhibitor in an aggressive medium. From our definition, suppose the inhibition efficiency at an initial temperature, T_1 is I_0 , and the inhibition efficiency at a new temperature T_2 is I_T , then the fractional change in inhibition efficiency per initial inhibition efficiency per Kelvin rise in temperature is described as the temperature coefficient of corrosion inhibition efficiency, μ , such that

$$(I_T - I_0)/I_0\Delta T = \mu \quad (15)$$

This equation rearranges to become

$$I_T = I_0\mu\Delta T + I_0 \quad (16)$$

A plot of I_T against change in temperature, ΔT , therefore should yield a straight line with slope equal to $I_0\mu$ and intercept equal to I_0 as shown in figure 8 below. This equation is derived using the concept of temperature coefficient of resistance [a popular concept of classical physics] where the extent of change in resistance of a wire with measureable changes in temperature has been quantitatively defined. Table 6 shows the calculated values of μ for the inhibition of mild steel corrosion by different concentrations of zinc soap in the sulphuric acid solution both

in the absence and presence of 0.001 M KI. The negative values of μ so obtained indicate decrease in inhibition efficiency with increase in temperature. This observation is not reported anywhere in the field but is consistent with physical adsorption mechanism.

Table 6: Temperature coefficient of inhibition efficiency

| Conc (mg/L) | 2 | 4 | 6 | 8 | 10 |
|----------------------|--------|--------|--------|--------|--------|
| Zn soap alone | -0.547 | -0.637 | -0.630 | -0.621 | -0.612 |
| Zn soap + 0.001 M KI | -0.553 | -0.481 | -0.474 | -0.413 | -0.374 |

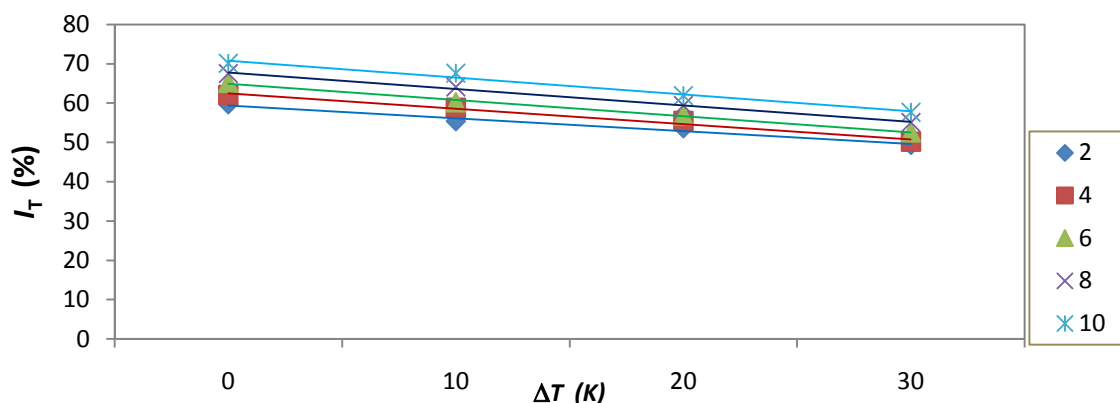


Fig 3 (a): Plot of I_T against ΔT for the inhibition of mild steel corrosion in 1.0 M H_2SO_4 by different concentrations of Zinc soap at 303 - 333 K

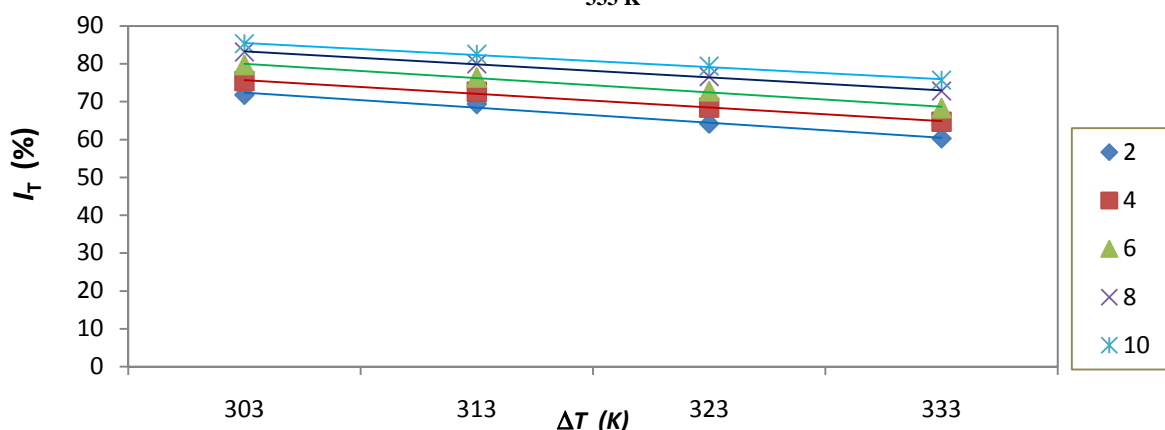


Fig 3 (b): Plot of I_T against ΔT for the inhibition of mild steel corrosion in 1.0 M H_2SO_4 by different concentrations of Zinc soap blended with 0.001 M KI at 303 - 333 K

3.4 Kinetic and Thermodynamic Consideration

Arrhenius equation provides a mathematical dependency between the reaction rates (this time, corrosion rate) and temperature as follows:

$$\log CR = \text{Log } A - E_a/2.303RT \tag{17}$$

where CR is the corrosion rate, A is the Arrhenius pre-exponential constant, R is the molar gas constant, and T is the absolute temperature. A plot of $\log CR$ against $1/T$ produces straight lines (figure 9) with slope as $(-E_a/2.303R)$ and intercept as $\log A$. Activation parameters calculated from the plot are displayed in table 7. The transition state equation (18) afforded thermodynamic parameters (table 7) such as enthalpy change, ΔH^*_{ads} and entropy change, ΔS^*_{ads} from a plot of $\log CR/T$ versus $1/T$ shown in figure 10.

$$v = RT/Nh \exp(\Delta S^*_{ads}/R) \exp(\Delta H^*_{ads}/RT) \tag{18}$$

where N is the Avogadro's number and h is the planks constant. The enthalpy was calculated from the slope $(-\Delta H^*_{ads}/2.303R)$ while the entropy was calculated from the intercept $\{ \ln(R/Nh)+ (\Delta S^*_{ads}/2.303R) \}$ of the plot.

On the basis of effects of temperature, inhibitors have been categorized into three viz:

- (i) Inhibitors showing a decrease in % I with increase in T ; $E_a(\text{uninhibited}) > E_a(\text{inhibited})$;
- (ii) Inhibitors showing no change in % I with variation in T ; E_a does not change with the presence and absence of inhibitors, and
- (iii) Inhibitors showing increase in % I with increase in T ; $E_a(\text{uninhibited}) > E_a(\text{inhibited})$

A decrease in % I with increase in temperature was obtained and may be ascribed to a shift in the adsorption-desorption equilibrium towards desorption of adsorbed inhibitor due to increased solution agitation [22]. This observation suggests that the adsorption of the Zn soap onto the steel surface is physical in nature. Invariably, an increase in solution temperature decreases the number of adsorbed inhibitor molecules, resulting in appreciable desorption and thus, a decrease in inhibition efficiency.

Inhibitors may affect the inhibition efficiency in two possible mechanisms: either by decreasing the available acid attack surface area of the metal (geometric blocking effect) or by modifying (increasing) the activation energy of the anodic or cathodic reactions occurring in the inhibitor-free surface [24]. The higher activation energies depict increased energy barrier, slow reaction and sensitivity of reaction rate to temperature variations. Physical adsorption is associated with larger E_a values of the inhibited solution than that of the free acid solution [25]. Therefore, decrease in % I with increasing temperature and $E_a(\text{inhibited}) > E_a(\text{free acid solution})$ probably shows that Zn-soap inhibited the acid corrosion process via physical adsorption. As concentration of Zn-soap increases, the number of molecules per volume of solution increases, the number of active sites on the metal surface “blanketed” by the inhibitor molecule increases, thus raising the minimum energy required by the acid to attack those sites (i.e. E_a), with the possibility of formation of adsorptive film with electrostatic character.

Like E_a , the ΔH_{ads} increases with increase in concentration of the inhibitor. The negative values denote the exothermic nature of the adsorption process. The negative entropy ($-\Delta S^0$) increases gradually with the presence of the inhibitor compared to that of the uninhibited solution, indicating the formation of ordered stable layer of inhibition on the steel surface [22, 26].

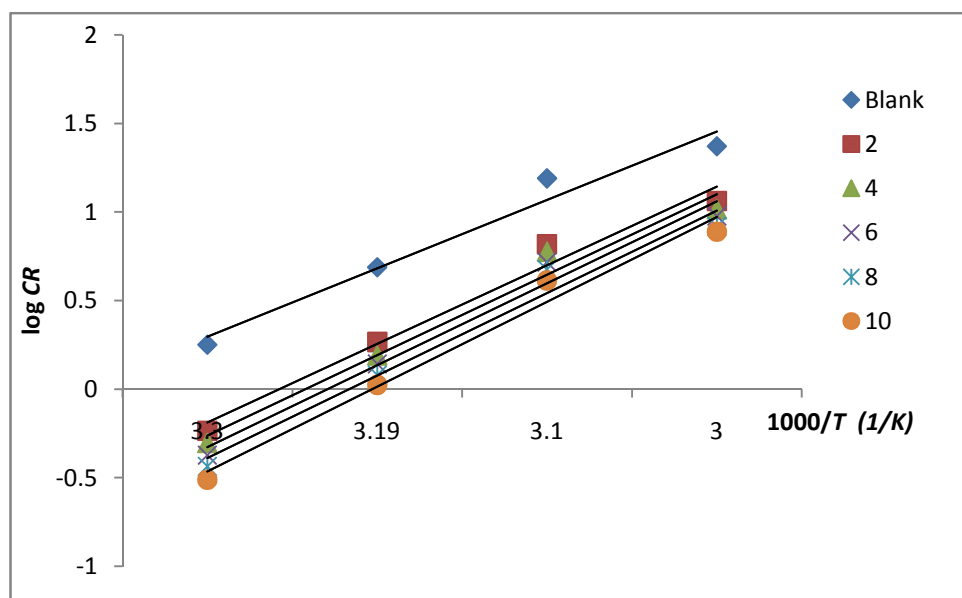


Fig 9 (a): Arrhenius plot for the adsorption behavior of different concentrations of metallic soap of zinc at sulphuric acid-mild steel interface at 303 – 333 K

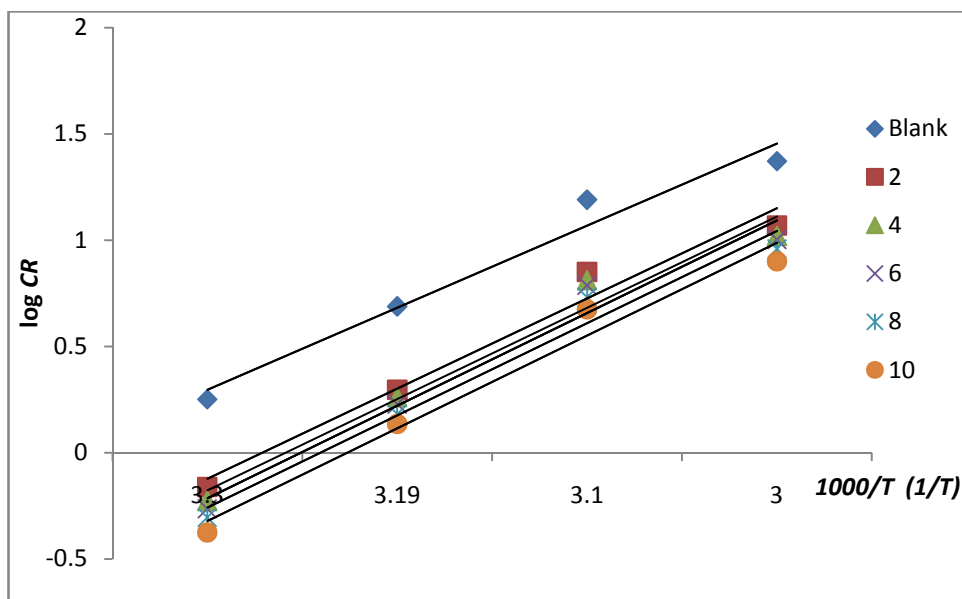


Fig 9 (b): Arrhenius plot for the adsorption behavior of different concentrations of metallic soap of zinc containing 0.001 M KI at sulphuric acid-mild steel interface at 303 – 333 K

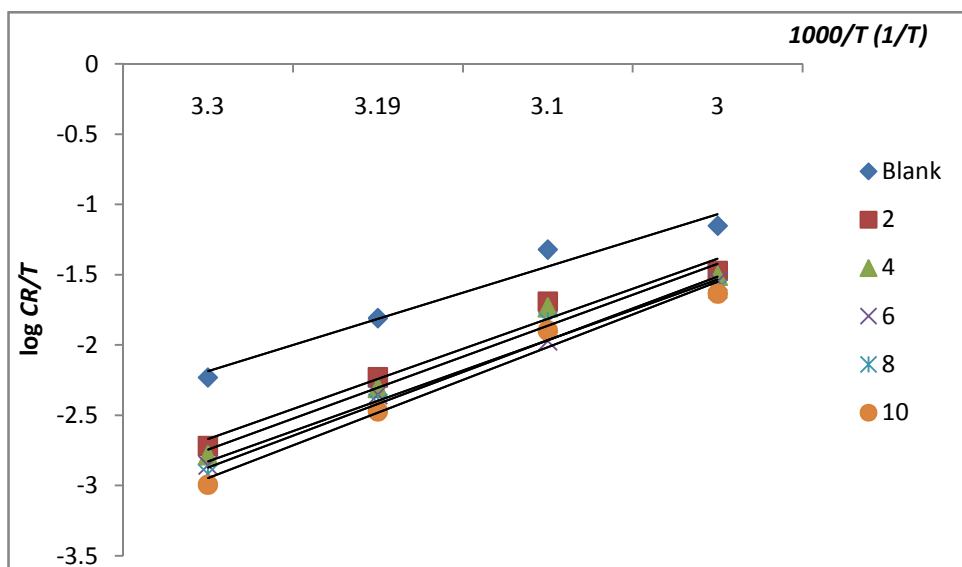


Fig 10 (a): Transition state plot for the adsorption behavior of different concentrations of metallic soap of zinc at sulphuric acid-mild steel interface at 303 – 333 K

Table 7: Kinetic/ Thermodynamic Parameters

| Systems | Ea (kJ/mol) | A (x 10 ⁻⁴) | ΔH _{ads} (kJ/mol) | ΔS _{ads} (kJ/mol) |
|---------------------|-------------|-------------------------|----------------------------|----------------------------|
| Blank | 7.41 | 8.00 | -3.03 | -234.79 |
| 2mg/L Zn soap | 8.02 | 3.05 | -3.37 | -247.37 |
| 4mg/L Zn soap | 8.17 | 2.75 | -3.43 | -247.70 |
| 6mg/L Zn soap | 8.29 | 2.51 | -3.46 | -247.91 |
| 8mg/L Zn soap | 8.31 | 2.37 | -3.52 | -248.28 |
| 10mg/L Zn soap | 8.40 | 2.11 | -3.53 | -248.79 |
| 2mg/L Zn soap + KI | 8.40 | 2.00 | -3.57 | -248.99 |
| 4mg/L Zn soap + KI | 8.44 | 1.74 | -3.58 | -249.61 |
| 6mg/L Zn soap + KI | 8.61 | 1.43 | -3.63 | -250.11 |
| 8mg/L Zn soap + KI | 8.75 | 1.15 | -3.66 | -250.73 |
| 10mg/L Zn soap + KI | 8.80 | 1.01 | -3.69 | -251.27 |

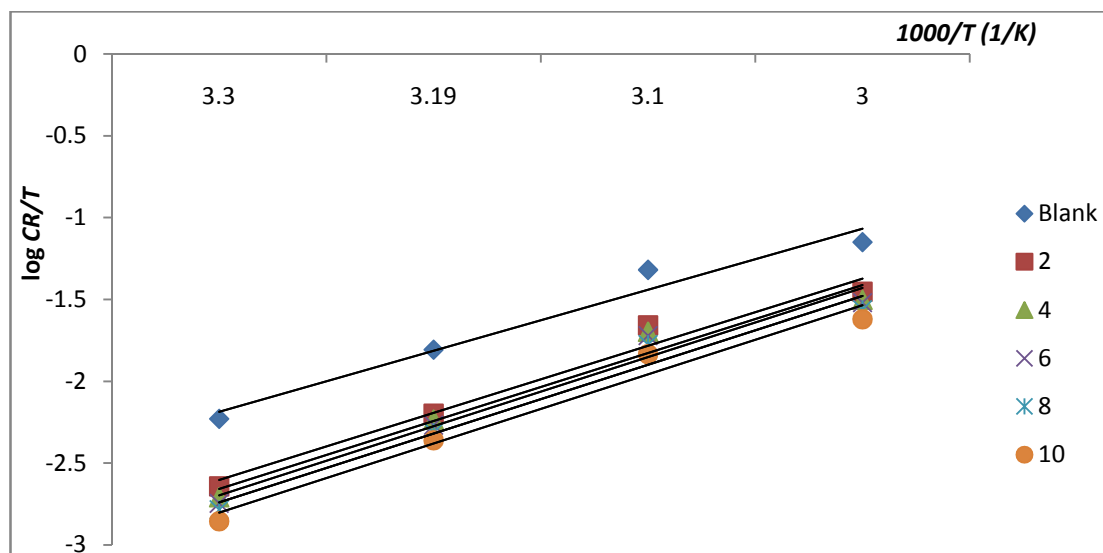


Fig 10 (a): Transition state plot for the adsorption behavior of different concentrations of metallic soap of zinc containing 0.001 M KI at sulphuric acid-mild steel interface at 303 – 333 K

CONCLUSION

On the basis of this study, the following conclusions have been drawn:

- The Zn-soap acts as an effective and efficient inhibitor for mild steel corrosion in sulphuric acid medium at all temperatures studied, being a better inhibitor at 303 K
- Corrosion rate increases as temperature increases both in the absence and presence of the inhibitor and decreases further in the presence of the inhibitor.
- Inhibition efficiency of Zn-soap increases with increase in its concentration but decreases with increase in temperature
- Addition of iodide ions further increased inhibition efficiency and thus reduced the corrosion rate.
- The corrosion inhibition is probably due to the adsorption of the inhibitor on to the mild steel surface and thus blocking the corrosion active sites by the physical adsorption mechanism
- The inhibition of mild steel corrosion by Zn-soap obeys modified Langmuir adsorption model at all the concentrations and temperatures studied
- The values of entropy of adsorption obtained indicate spontaneous adsorption and the instability of the adsorbed layer
- The adsorption process is exothermic as implicated by the values of the enthalpy of adsorption and there is more than one molecule of the fatty acids in the Zn-soap occupying the active sites of the metal at the metal-acid interface.
- The adsorption sites of the inhibitor constitutes mainly the carbonyl group, -OH group and C=C in the molecular structure of the fatty acid constituents of the inhibitor
- Temperature coefficient of inhibition efficiency is a reliable approach to elucidating the mechanism of adsorption of an inhibitor
- Metallic soap of zinc is a recommended additive as corrosion inhibitor for metal paints and polishes manufacturers as well as other chemical and petrochemical industries.

The equations 15 -16 above were derived and applied for the first time by one of the authors (Ekemini B. Ituen). It is dimensionally consistent and should be referred to as *Ekemini Ituen's temperature coefficient of inhibition efficiency equation* at anytime it is applied.

REFERENCES

- [1] Xianghong Li, Shuduan Deng, Hui Fu. *Corros. Sci.* **2010**, 53 (1): 302 -309.
- [2] Oguzie, E.E. *Corros. Sci.* **2007**, 49: 1527 –1539.
- [3] Oguzie, E. E. *Mater. Chem. Phys.* **2006**, 99 (2/3) 441-446.
- [4] Ebenso, E. E. *Nig. Corros. Journ.* **1998**, 1(1): 29-44.
- [5] Chao, P., Liang, Q., Li, Y.. *Appl. Surf. Sci.* **2005**, 1592-1596.
- [6] Ahamed, I and Quarashi, M. A. *Corros. Sci.* **2010**, 52: 651-656.
- [7] Ituen, E. B. and Udo, U. E. *Der Chimic. Sini.* **2012**, 3 (6): 1394-1405

- [8] Umoren, S. A., Ebenso, E. E., Ogbobe, E. *Journ. Appl. Polym. Sci.* **2009**, 113 (6): 3533-3543.
- [9] Okafor, P.C., Ikpi, M. E., Uwah, I. E., Ebenso, E.E., Ekpe, U.J., Umoren, S.A. *Corros. Sci.* **2008**, 50: 2310–2317.
- [10] Umoren, S.A, Ekanem, U.F. *Chem. Eng. Comm.* **2010**, 197 (10) : 1339 – 1356.
- [11] Essien, E.A., Umoren, S.A., Essien, E. E., Udoh, A. P. *J. Mater. Environ. Sci.* **2012**, 3 (2): 477-484.
- [12] Ekpa, O. D., Fubara, E. P. and Morah, E. N. *I. J. Sci. Foo. Agric.* **1994**, 64: 483 – 486.
- [13] Steele, I. B. *J. Electrochem. Socie.* **2001**, 16: 81-86.
- [14] Austin, G. T. *Shreve's Chemical Processes Industries*. 5th ed., New York: McGraw – Hill Book Company, **2004**, 135-151.
- [15] Ekpa, O. D. and Ibok, U. J. *Troip. J. Appl. Sci.* **1991**, 1(1): 53 – 55.
- [16] Payne, H. F. *Organic Coating Technology*. Vol 2, Kampier: Vikkas Publishing House. **1998**, 231-283.
- [17] N.O. Obi-Egbedi, and I.B.Obot. *Arab. Journ. Chem.* **2010**, 5 (1): 121-133
- [18] Umoren, S. A., Obot, I. B., Obi-Egbedi, N. O. *J mater. Sci.* 2009, 44 : 274-279
- [19] U.M. Eduok, S.A. Umoren, A.P. Udoh. *Arab. Journ. Chem.* 2010, doi: 10.1016/j.arabjc.2010.09.006
- [20] Abdel-Gaber, A.M., Abd-El-Nabey, B.A., Sidahmed, I.M., El-Zaya-dy, A.M., Saadawy, M. *Corros. Sci.* **2006**, 48: 2765–2779.
- [21] R.F.V. Villamil, P. Corio, J.C. Rubin, S.M.L. Agostinho. *J. Electroanal. Chem.* **1999**, 472: 112.
- [22] Ituen, E. B., Odozi, N. W., Udo, U.E., Dan, E. U. *IOSR-J. Appl. Chem.* **2013**, 3 (4): 52-59
- [23] Popova, A., Sokolova, E., Raicheva, S., Christov, M. *Corros. Sci.* **2003**, 45: 33–58
- [24] Umoren, S. A., Ogbobe, O., Igwe, I. O., Ebenso, E. E. *Corros. Sci.* **2008**, 50: 1998-2006.
- [25] Martinez, S. and Stern, I. *J. Appli. Electrochem.* **2001**, 31 (9): 973-978.
- [26] Ostovan, A., Hoseinieh, S. M., Shadrzadeh, S. R., Hashemi, S. J. *Corros. Sci.* **2009**, 51 (9): 1935-1949.
- [27] Dwivedi and Misra, 2010 A. Dwivedi and N. Misra, *Der Pharma Chem.* **2** (2) (2010), p. 58.

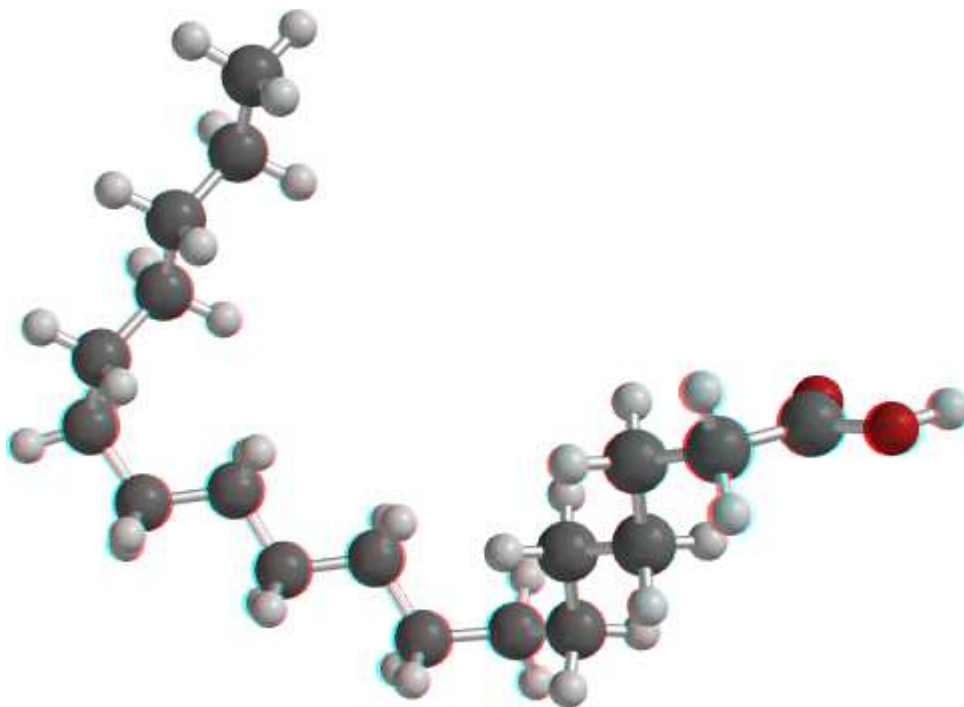


Figure 2 (a): Optimized structure of stearic acid using DFT at the B3LYP/6-31G*basis set level

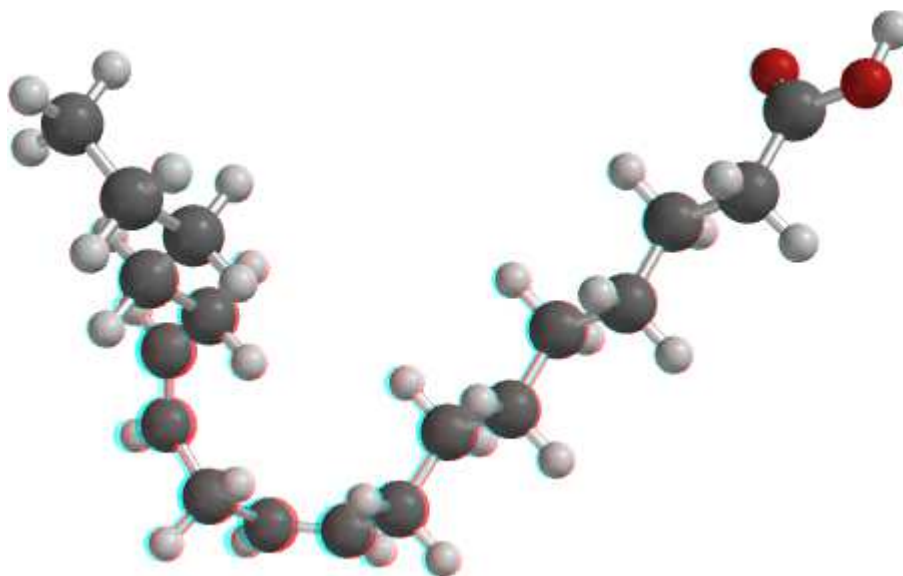


Figure 2 (b): Optimized structure of linoleic acid using DFT at the B3LYP/6-31G*basis set level

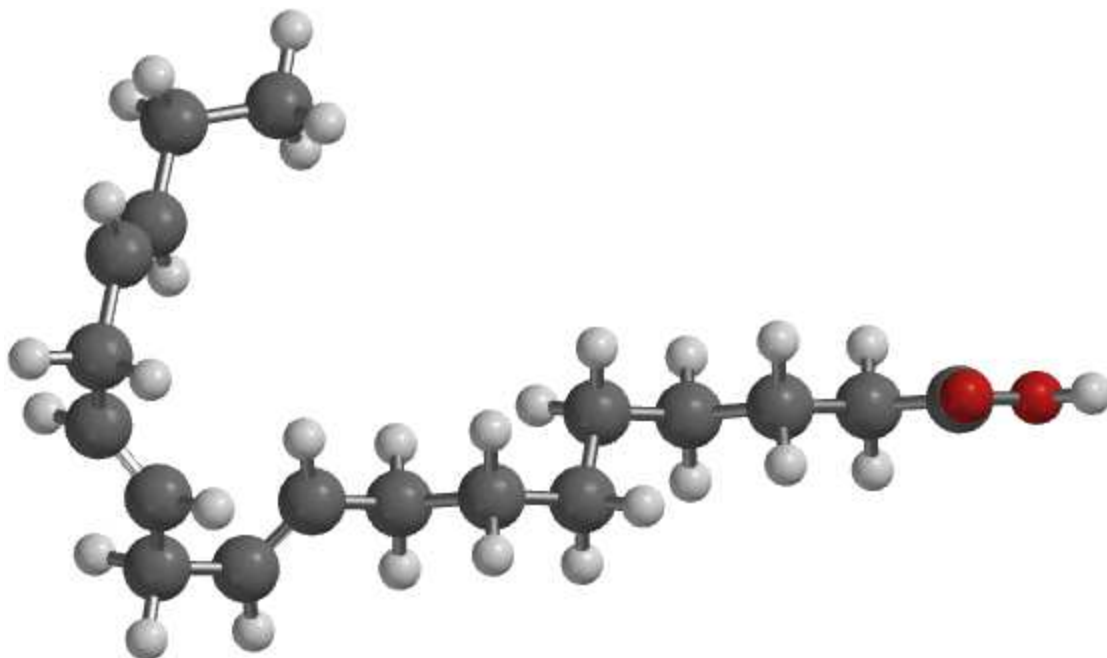


Figure 2 (c): Optimized structure of linolenic acid using DFT at the B3LYP/6-31G* basis set level

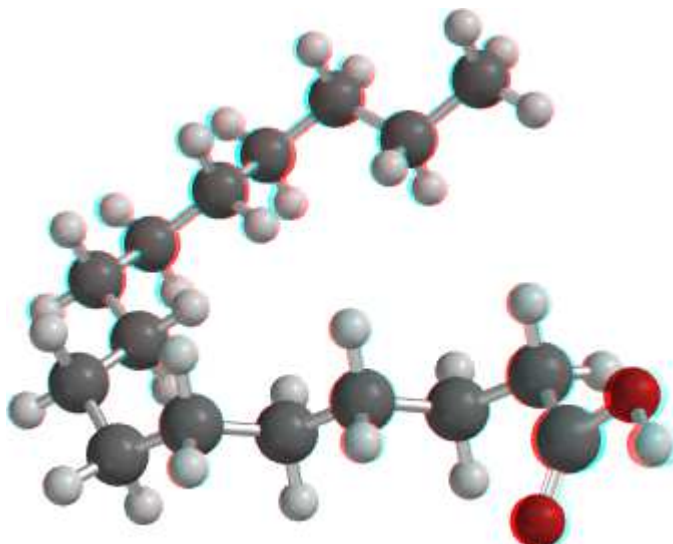


Figure 2 (d): Optimized structure of palmitic acid using DFT at the B3LYP/6-31G* basis set level

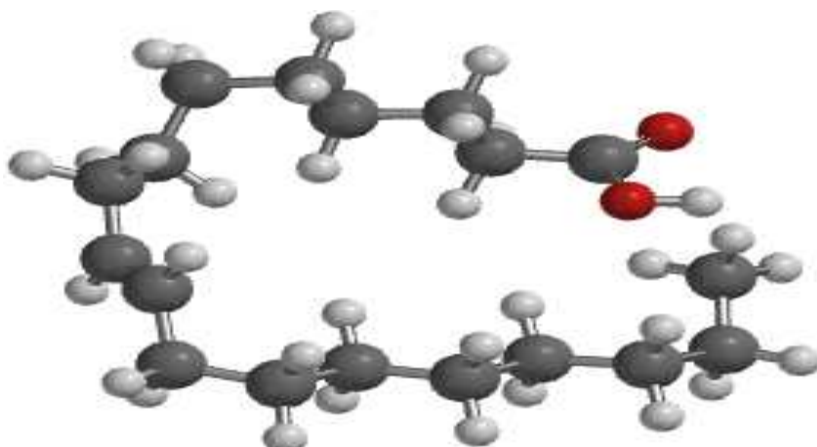


Figure 2 (e): Optimized structure of oleic acid using DFT at the B3LYP/6-31G* basis set level

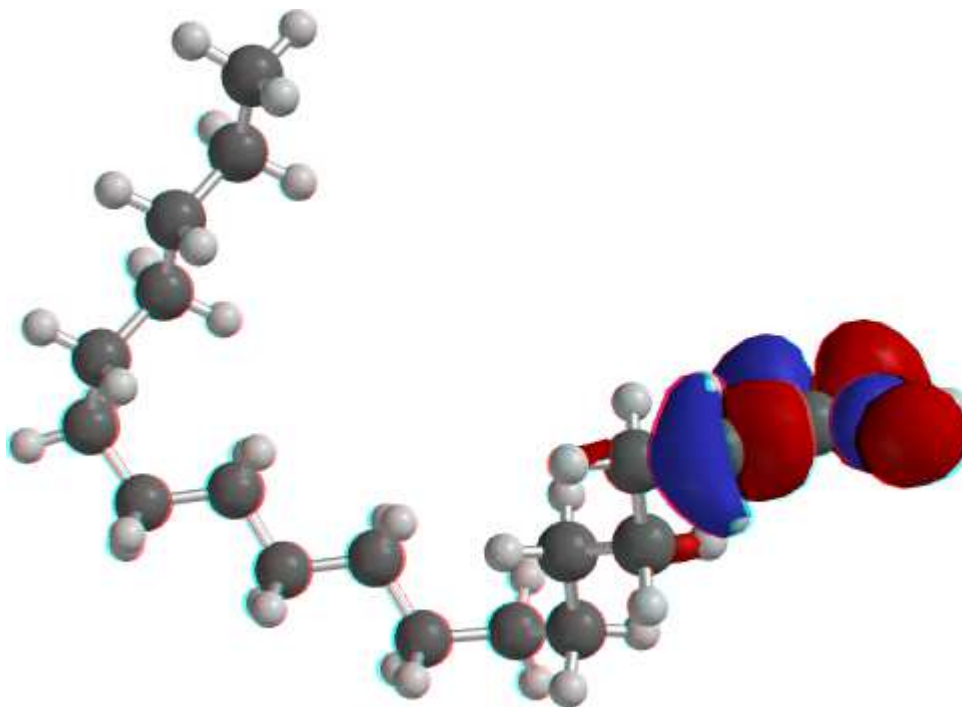


Figure 3(a). The highest occupied molecular orbital (HOMO) density of stearic acid using DFT at the B3LYP/6-31G*basis set level

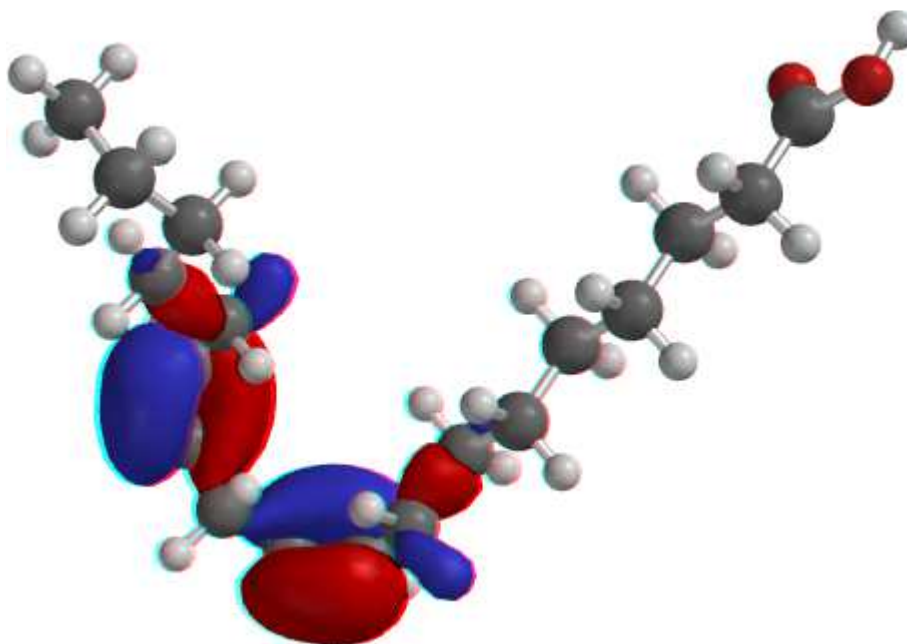


Figure 3(b): The highest occupied molecular orbital (HOMO) density of linoleic acid using DFT at the B3LYP/6-31G*basis set level

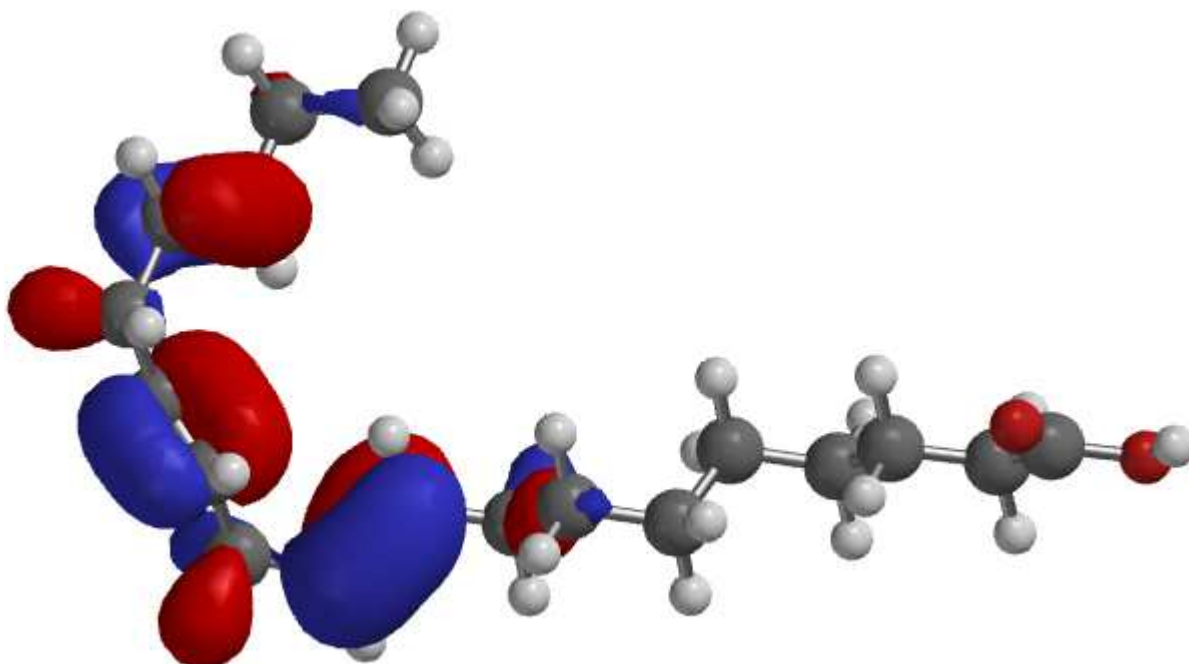


Figure 3(c): The highest occupied molecular orbital (HOMO) density of linolenic acid using DFT at the B3LYP/6-31G*basis set level

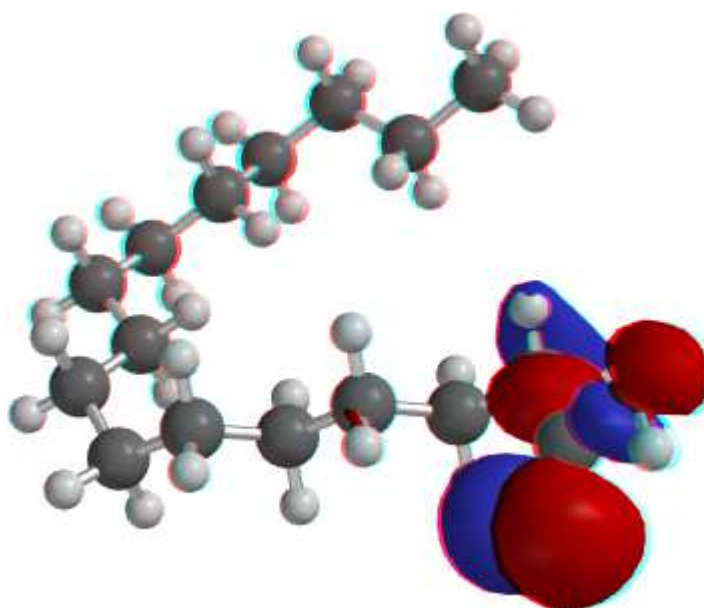


Figure 3(d): The highest occupied molecular orbital (HOMO) density of palmitic acid using DFT at the B3LYP/6-31G*basis set level

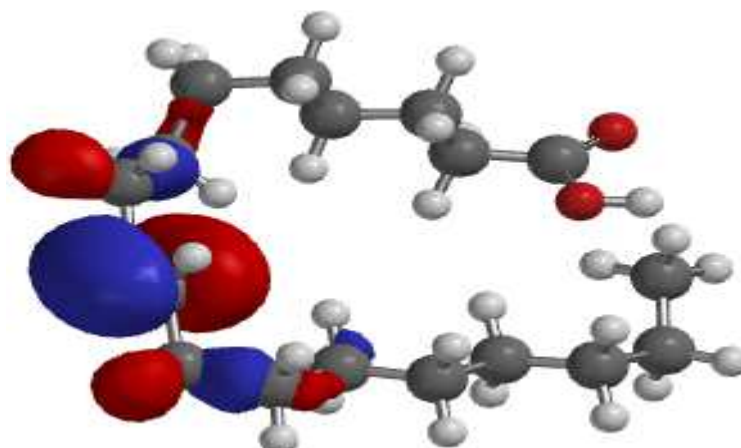


Figure 3(e): The highest occupied molecular orbital (HOMO) density of oleic acid using DFT at the B3LYP/6-31G*basis set level

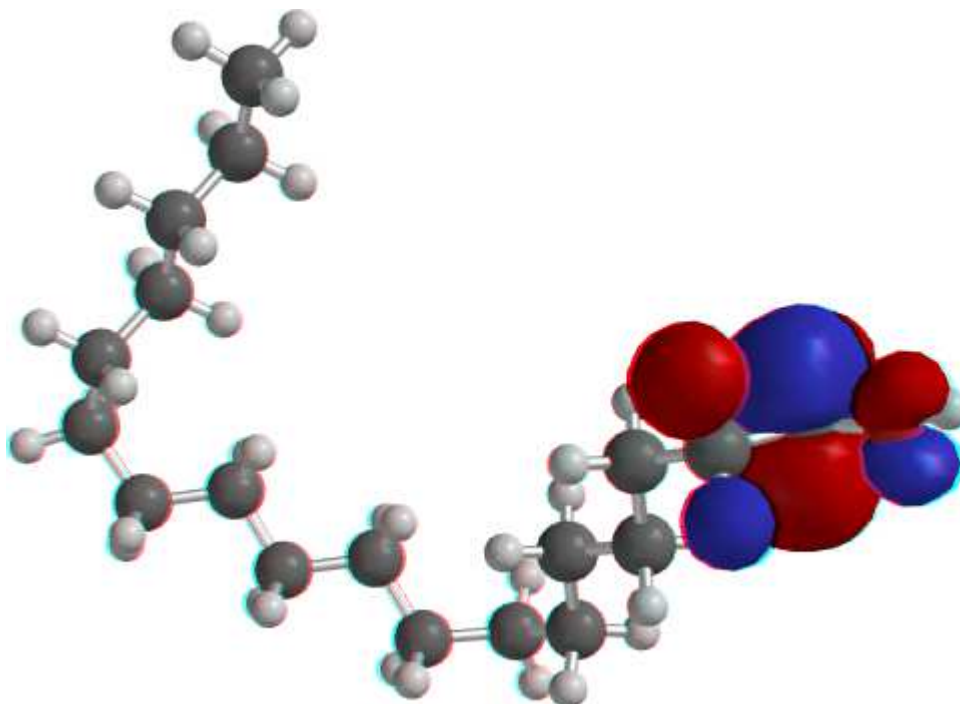


Figure 4(a): The Lowest unoccupied molecular orbital (LUMO) density of stearic acid using DFT at the B3LYP/6-31G* basis set level

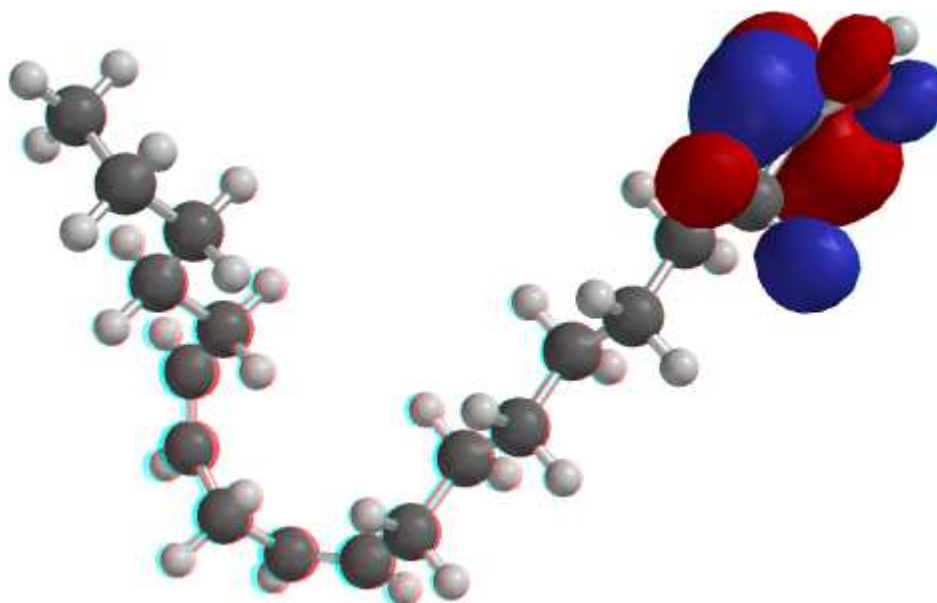


Figure 4(b): The Lowest unoccupied molecular orbital (LUMO) density of linoleic acid using DFT at the B3LYP/6-31G* basis set level

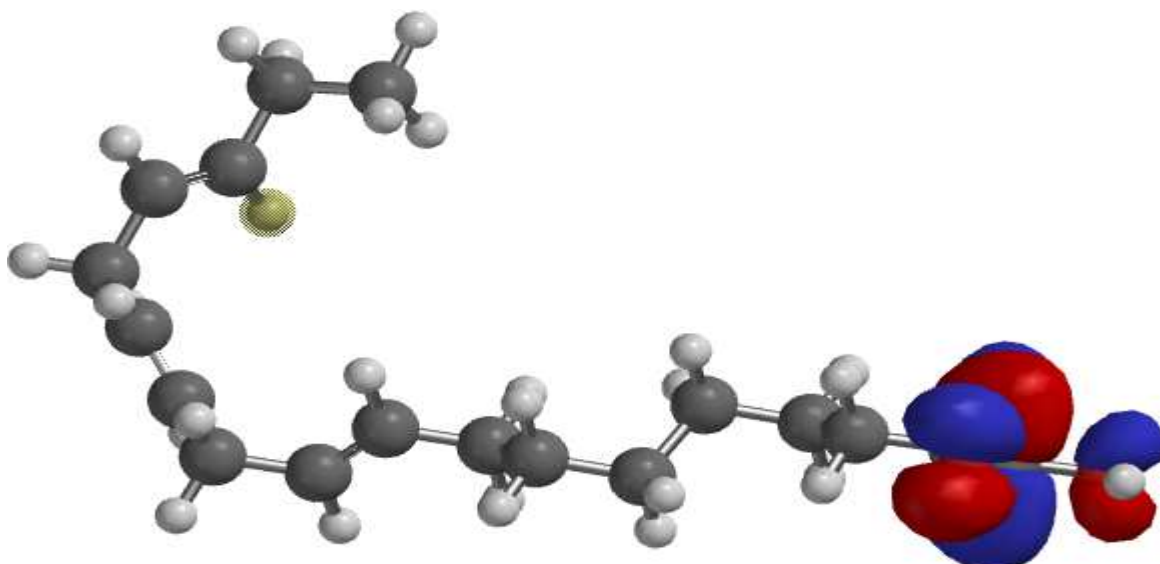


Figure 4(c): The Lowest unoccupied molecular orbital (LUMO) density of linolenic acid using DFT at the B3LYP/6-31G* basis set level

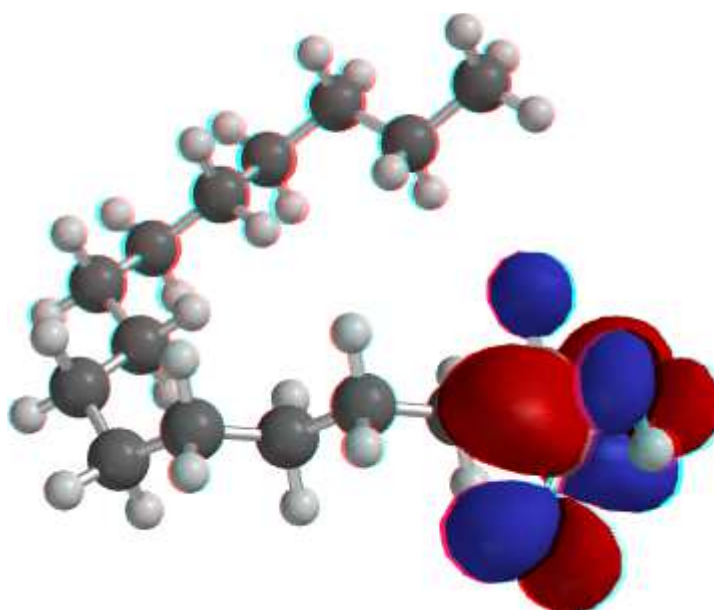


Figure 4(d): The Lowest unoccupied molecular orbital (LUMO) density of palmitic acid using DFT at the B3LYP/6-31G* basis set level

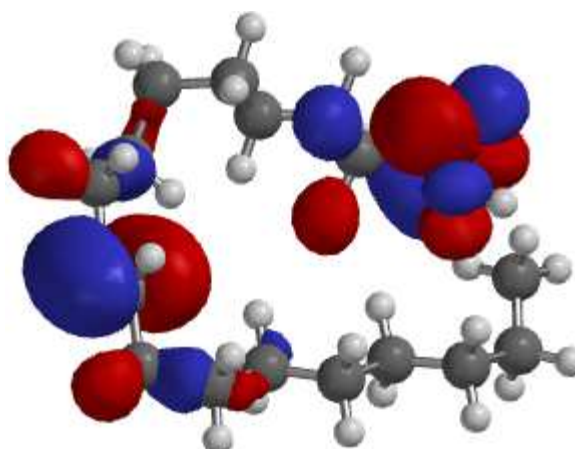


Figure 4(e): The Lowest unoccupied molecular orbital (LUMO) density of oleic acid using DFT at the B3LYP/6-31G* basis set level

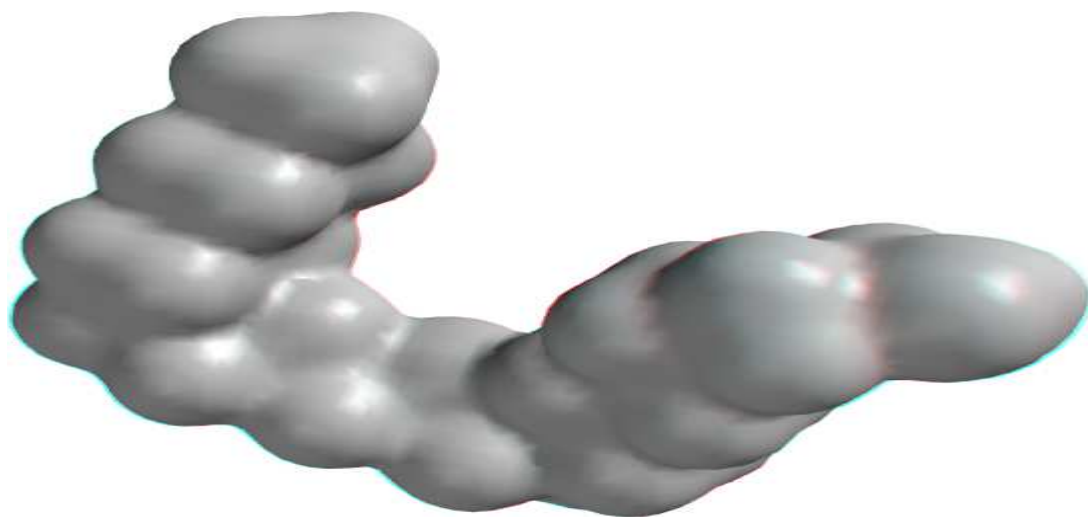


Figure 5(a). The density of stearic acid using DFT at the B3LYP/6-31G* basis set level

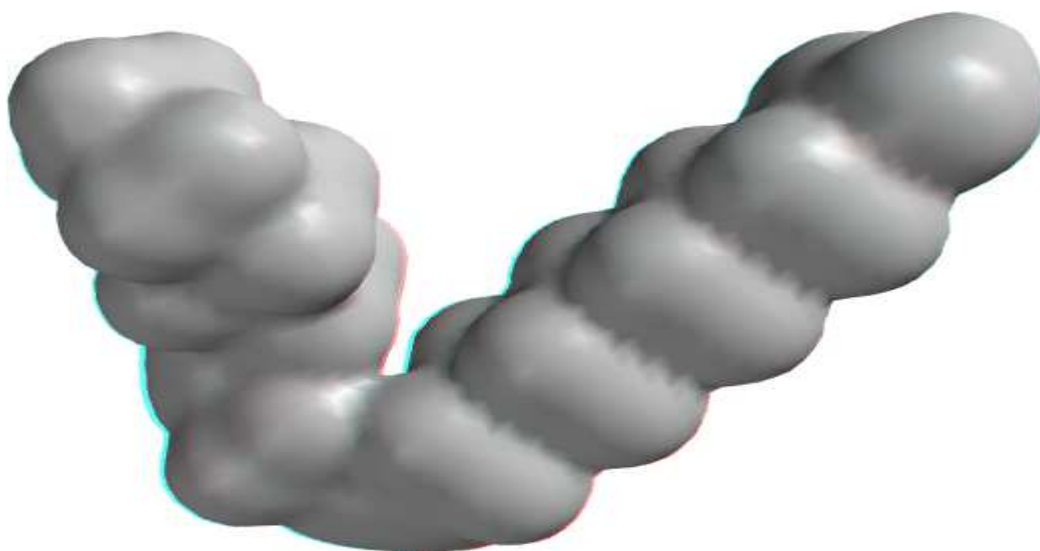


Figure 5(b): The density of linoleic acid using DFT at the B3LYP/6-31G* basis set level

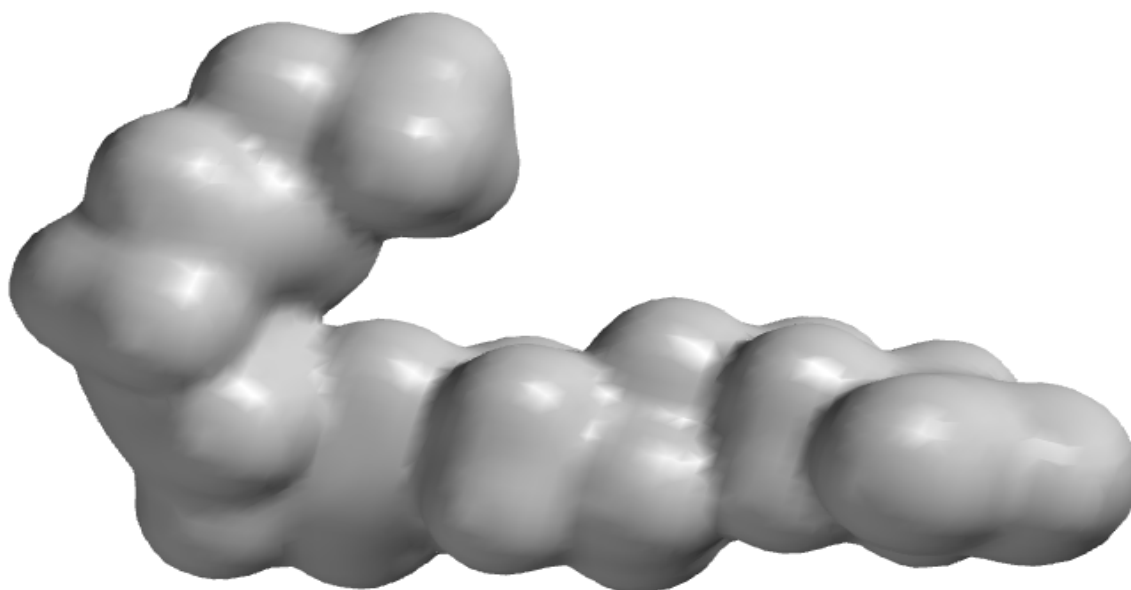


Figure 5(c). The density of linolenic acid using DFT at the B3LYP/6-31G* basis set level

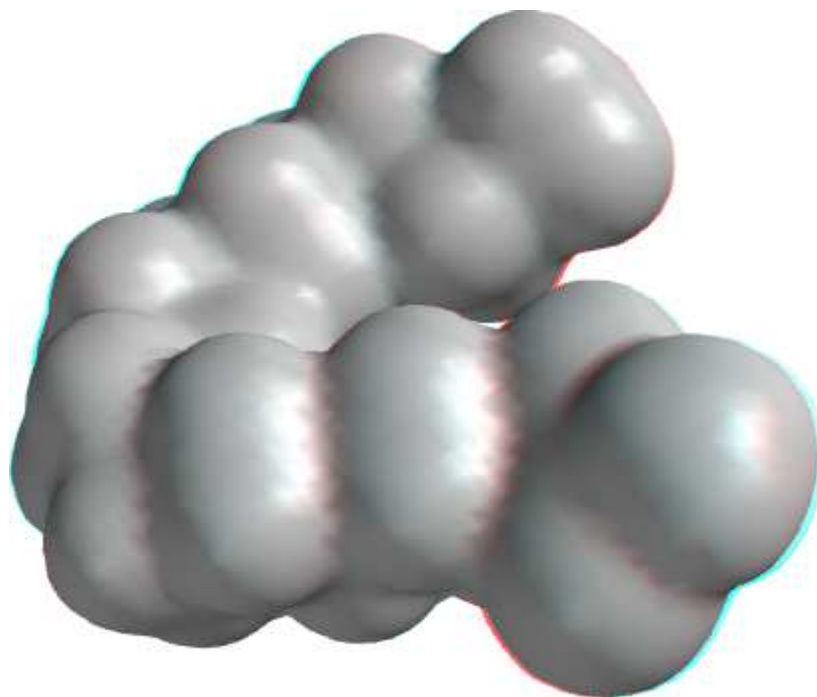


Figure 5 (d): The density of palmitic acid using DFT at the B3LYP/6-31G*basis set level

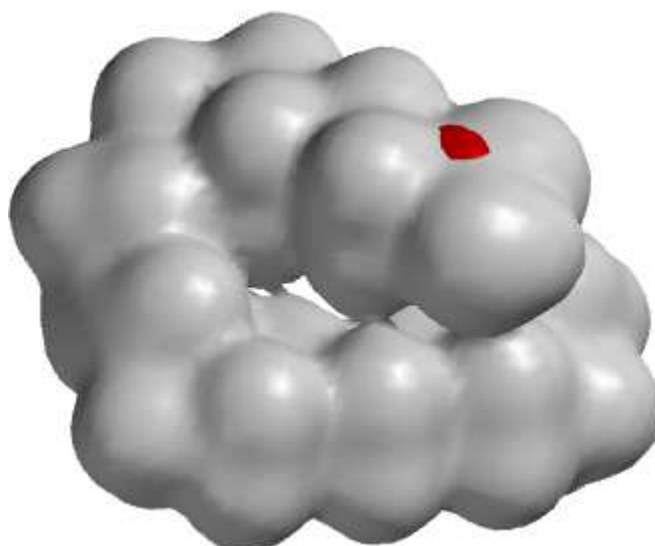


Figure 5(e): The density of oleic acid using DFT at the B3LYP/6-31G*basis set level

Table 3(a): Some molecular properties of stearic acid calculated using DFT at the B3LYP/6-31G* basis set level

| MOLECULAR PARAMETER | CACULATED VALUE (eV) |
|---------------------|----------------------|
| $E_{(HOMO)}$ | -7.47 |
| $E_{(LUMO)}$ | 0.29 |
| ΔE | 7.76 |
| TOTAL ENERGY | -23348.68936 |
| DIPOLE MOMENT | 1.26 Debye |

Table 3(b): Some molecular properties of linoleic acid calculated using DFT at the B3LYP/6-31G* basis set level

| MOLECULAR PARAMETER | CACULATED VALUE (eV) |
|---------------------|----------------------|
| $E_{(HOMO)}$ | -6.30 |
| $E_{(LUMO)}$ | 0.33 |
| ΔE | 6.63 |
| TOTAL ENERGY | -23281.75265 |
| DIPOLE MOMENT | 1.78 Debye |

Table 3(c): Some molecular properties of linolenic acid calculated using DFT at the B3LYP/6-31G* basis set level

| MOLECULAR PARAMETER | CACULATED VALUE (eV) |
|---------------------|----------------------|
| E _(HOMO) | -6.31 |
| E _(LUMO) | 0.33 |
| TOTAL ENERGY | -23249.5177 |
| ΔE | 6.64 |
| DIPOLE MOMENT | 1.32 debye |

Table 3(d): Some molecular properties of palmitic acid calculated using DFT at the B3LYP/6-31G* basis set in ethanol

| MOLECULAR PARAMETER | CACULATED VALUE (eV) |
|---------------------|----------------------|
| E _(HOMO) | -7.46 |
| E _(LUMO) | 0.30 |
| ΔE | 7.76 |
| TOTAL ENERGY | -21209.30056 |
| DIPOLE MOMENT | 1.28 debye |

Table 3(e): Some molecular properties of oleic acid calculated using DFT at the B3LYP/6-31G* basis set level

| MOLECULAR PARAMETER | CACULATED VALUE (eV) |
|---------------------|----------------------|
| E _(HOMO) | -6.43 |
| E _(LUMO) | 0.24 |
| ΔE | 6.67 |
| TOTAL ENERGY | -23316.43 |
| DIPOLE MOMENT | 1.40 debye |

Table 4 (a): Mullikan charge distribution of stearic acid calculated using DFT at the B3LYP/6-31G* basis set level

| | | | | | | | | | | |
|--------|--------|--------|--------|--------|--------|--------|--------|--------|--------|--------|
| ATOM | C1 | O1 | O2 | H2 | C2 | H1 | H4 | C3 | H5 | H6 |
| CHARGE | +0.579 | -0.464 | -0.569 | +0.407 | -0.354 | +0.171 | +0.177 | -0.252 | +0.154 | +0.130 |
| ATOM | C4 | H3 | H7 | C5 | H9 | H10 | C6 | H8 | H11 | C7 |
| CHARGE | -0.262 | +0.122 | +0.152 | -0.254 | +0.133 | +0.132 | -0.255 | +0.125 | +0.129 | -0.260 |
| ATOM | H12 | H13 | C8 | H14 | H15 | C9 | H16 | H18 | C10 | H17 |
| CHARGE | +0.128 | +0.128 | -0.253 | +0.125 | +0.127 | -0.259 | +0.135 | +0.127 | -0.254 | +0.125 |
| ATOM | H19 | C11 | H20 | H22 | C12 | H21 | H23 | C13 | H25 | H26 |
| CHARGE | +0.126 | -0.253 | +0.133 | +0.127 | -0.255 | +0.126 | +0.126 | -0.260 | +0.128 | +0.128 |
| ATOM | C14 | H24 | H27 | C15 | H29 | H30 | C16 | H28 | H31 | C17 |
| CHARGE | -0.254 | +0.127 | +0.127 | -0.260 | +0.126 | +0.137 | -0.246 | +0.125 | +0.125 | -0.247 |
| ATOM | H32 | H34 | C18 | H33 | H35 | H36 | | | | |
| CHARGE | +0.130 | +0.130 | -0.441 | +0.140 | +0.141 | +0.141 | | | | |

Table 4(b): Mullikan charge distribution of linoleic acid calculated using DFT at the B3LYP/6-31G* basis set level

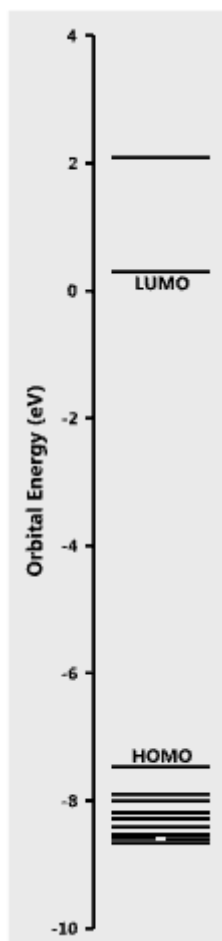
| | | | | | | | | | | | |
|--------|--------|--------|--------|--------|--------|--------|--------|--------|--------|--------|--------|
| ATOM | C1 | O1 | O2 | H2 | C2 | H1 | H4 | C3 | H3 | H5 | C4 |
| CHARGE | +0.577 | -0.462 | -0.572 | +0.407 | -0.355 | +0.173 | +0.174 | -0.249 | +0.149 | +0.150 | -0.258 |
| ATOM | H6 | H8 | C5 | H7 | H9 | C6 | H10 | H12 | C7 | H11 | H13 |
| CHARGE | +0.128 | +0.128 | -0.254 | +0.131 | +0.131 | -0.254 | +0.127 | +0.127 | -0.253 | +0.130 | +0.142 |
| ATOM | C8 | H14 | H16 | C9 | H17 | C10 | H15 | C11 | H18 | H19 | C12 |
| CHARGE | -0.302 | +0.136 | +0.135 | -0.103 | +0.118 | -0.094 | +0.119 | -0.348 | +0.145 | +0.149 | -0.100 |
| ATOM | H21 | C13 | H20 | C14 | H22 | H23 | C15 | H24 | H26 | C16 | H25 |
| CHARGE | +0.119 | -0.097 | +0.117 | -0.304 | +0.139 | +0.136 | -0.253 | +0.135 | +0.134 | -0.249 | +0.126 |
| ATOM | H27 | C17 | H29 | H30 | C18 | H28 | H31 | H32 | | | |
| CHARGE | +0.126 | -0.248 | +0.130 | +0.130 | -0.433 | +0.140 | +0.142 | +0.147 | | | |

Table 4 (c): Mullikan charge distribution of linolenic acid calculated using DFT at the B3LYP/6-31G* basis set level

| | | | | | | | | | | |
|--------|--------|--------|--------|--------|--------|--------|--------|--------|--------|--------|
| ATOM | C1 | O1 | O2 | H2 | C2 | H3 | H4 | C3 | H1 | H5 |
| CHARGE | +0.576 | -0.462 | -0.571 | +0.407 | -0.354 | +0.174 | +0.173 | -0.251 | +0.148 | +0.156 |
| ATOM | C4 | H7 | H8 | C5 | H6 | H10 | C6 | H11 | H12 | C7 |
| CHARGE | -0.60 | +0.127 | +0.128 | +0.258 | +0.129 | +0.134 | -0.259 | +0.138 | +0.125 | -0.255 |
| ATOM | H9 | H13 | C8 | H15 | H16 | C9 | H14 | C10 | H20 | C11 |
| CHARGE | +0.130 | +0.136 | -0.305 | +0.132 | +0.142 | -0.082 | +0.129 | -0.260 | +0.114 | -0.340 |
| ATOM | H18 | H22 | C12 | H21 | C13 | H23 | C14 | H26 | H28 | C15 |
| CHARGE | +0.151 | +0.146 | -0.095 | +0.124 | -0.097 | +0.124 | -0.341 | +0.147 | +0.151 | -0.122 |
| ATOM | H27 | C16 | H31 | C17 | H29 | H34 | C18 | H33 | H35 | H36 |
| CHARGE | +0.114 | -0.079 | +0.127 | -0.297 | +0.140 | +0.137 | -0.439 | +0.142 | +0.143 | 0.149 |

Table 4 (d): Mullikan charge distribution of palmitic acid calculated using DFT at the B3LYP/6-31G* basis set level

| | | | | | | | | | | |
|--------|--------|--------|--------|--------|--------|--------|--------|--------|--------|--------|
| ATOM | C1 | O1 | O2 | H2 | C2 | H1 | H4 | C3 | H5 | H6 |
| CHARGE | +0.579 | -0.464 | -0.568 | +0.407 | -0.354 | +0.170 | +0.177 | -0.252 | +0.155 | +0.131 |
| ATOM | C4 | H3 | H7 | C5 | H9 | H10 | C6 | H8 | H11 | C7 |
| CHARGE | -0.261 | +0.122 | +0.151 | -0.261 | +0.133 | +0.133 | -0.255 | +0.126 | +0.132 | -0.260 |
| ATOM | H12 | H13 | C8 | H14 | H15 | C9 | H16 | H18 | C10 | H17 |
| CHARGE | +0.129 | +0.128 | -0.255 | +0.126 | +0.126 | -0.255 | +0.141 | +0.125 | -0.255 | +0.126 |
| ATOM | H19 | C11 | H21 | H22 | C12 | H20 | H24 | C13 | H25 | H26 |
| CHARGE | +0.127 | -0.254 | +0.126 | +0.126 | -0.256 | +0.124 | +0.137 | -0.255 | +0.127 | +0.126 |
| ATOM | C14 | H23 | H27 | C15 | H28 | H30 | C16 | H29 | H31 | H32 |
| CHARGE | -0.247 | +0.125 | +0.126 | -0.247 | +0.133 | +0.129 | -0.441 | +0.141 | +0.142 | +0.139 |

**Figure 6 (a): Orbital energies (HOMO and LUMO) of stearic acid using DFT at the B3LYP/6-31G*basis set level**

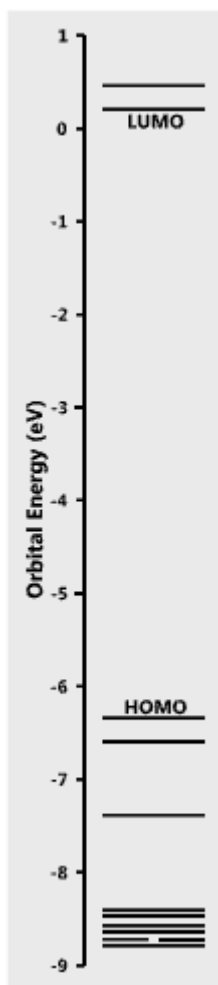


Figure 6 (b): Orbital energies (HOMO and LUMO) of linoleic acid using DFT at the B3LYP/6-31G* basis set level

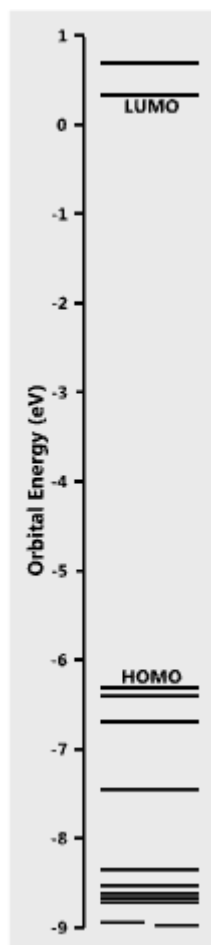


Figure 6 (c): Orbital energies (HOMO and LUMO) of linolenic acid using DFT at the B3LYP/6-31G*basis set level

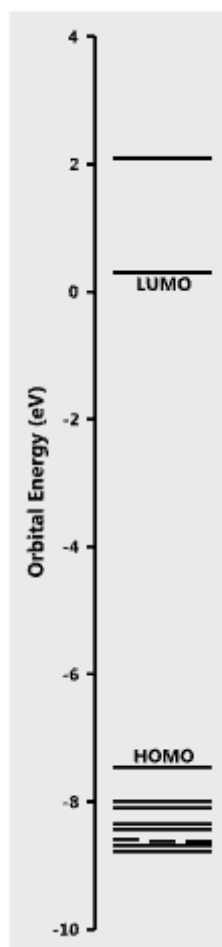


Figure 6 (d): Energies orbital (LUMO and HOMO) of palmitic acid using DFT at the B3LYP/6-31G*basis set level

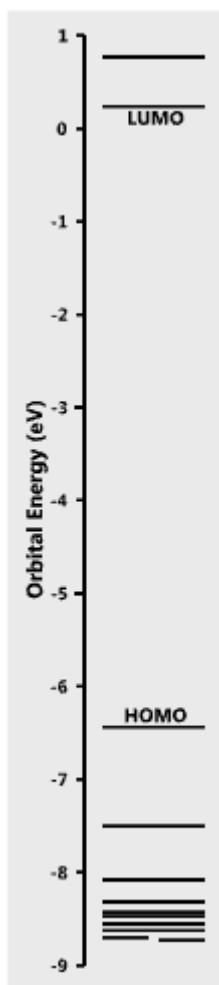


Figure 6 (e): Orbital energies(HOMO and LUMO) of oleic acid using DFT at the B3LYP/6-31G* basis set level

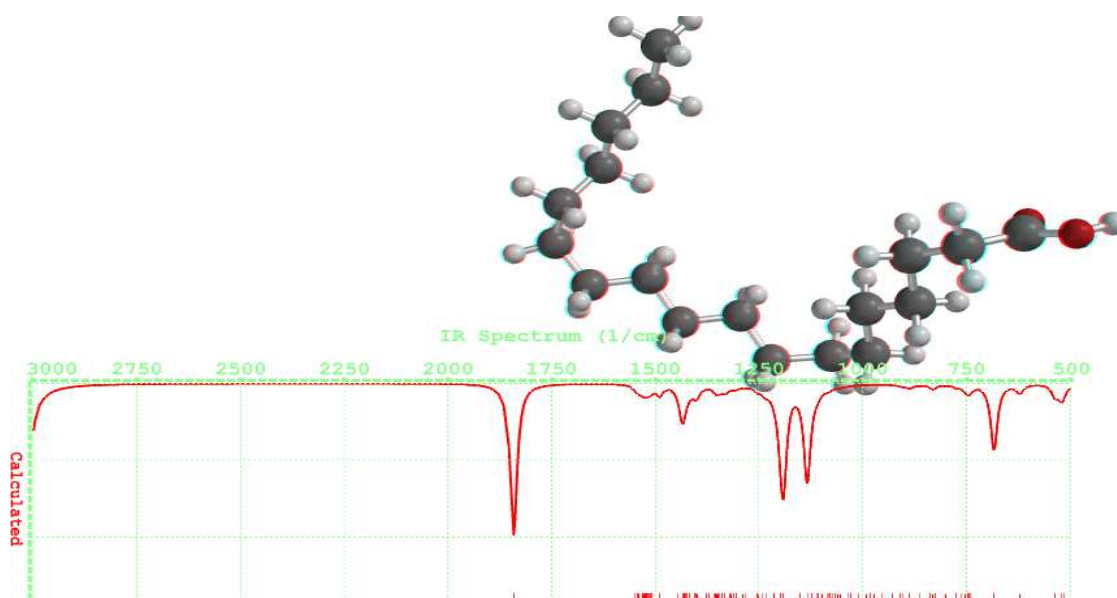


Figure 7(a): Infra-red spectra of stearic acid using DFT at the B3LYP/6-31G* basis set level

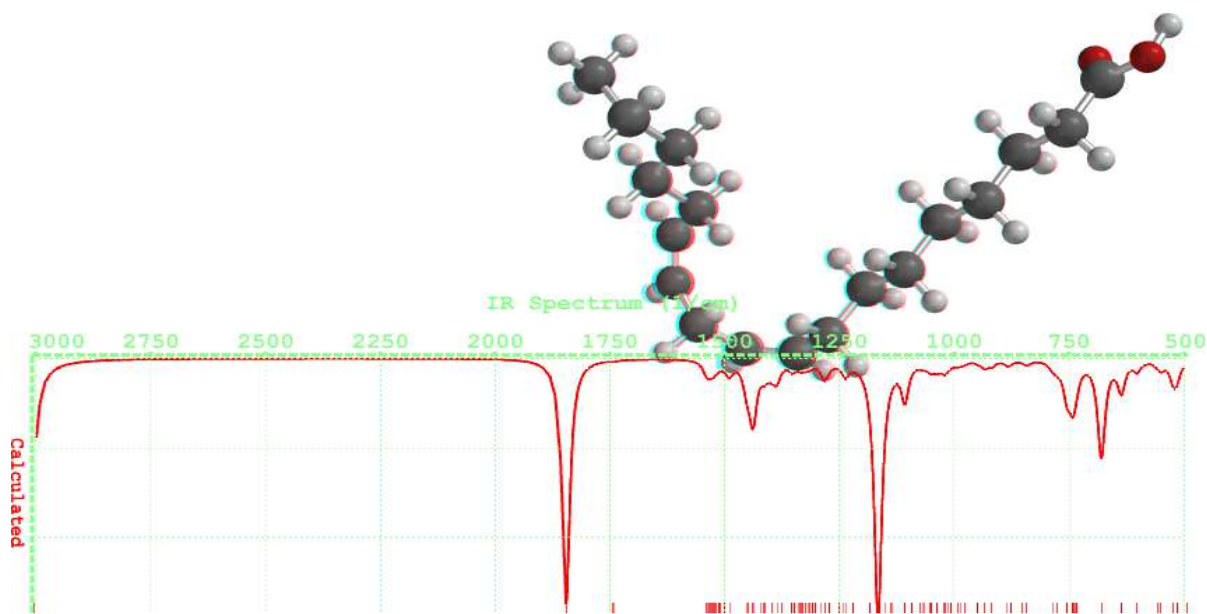


Figure 7(b): Infra-red spectra of linoleic acid using DFT at the B3LYP/6-31G* basis set level

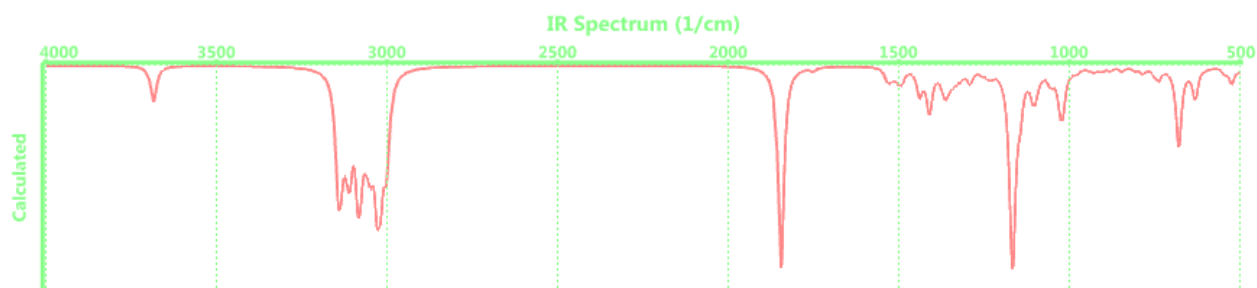


Figure 7(c): Infra-red spectra of linolenic acid using DFT at the B3LYP/6-31G* basis set level

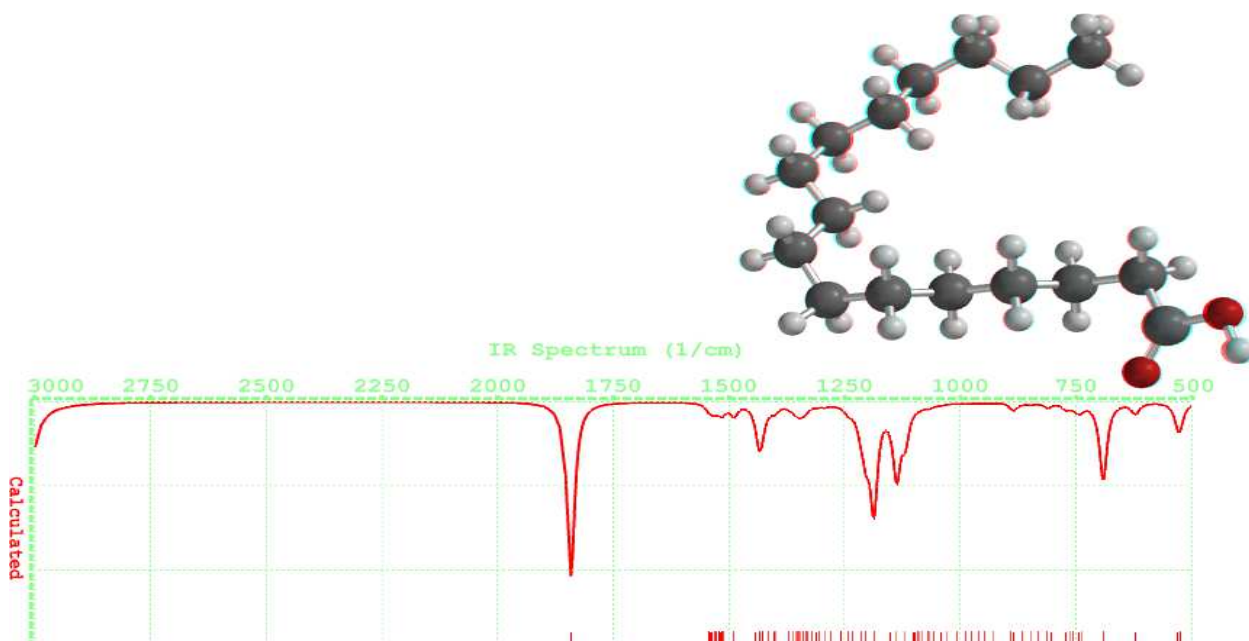


Figure 7(d): Infra-red spectra of palmitic acid using DFT at the B3LYP/6-31G* basis set level

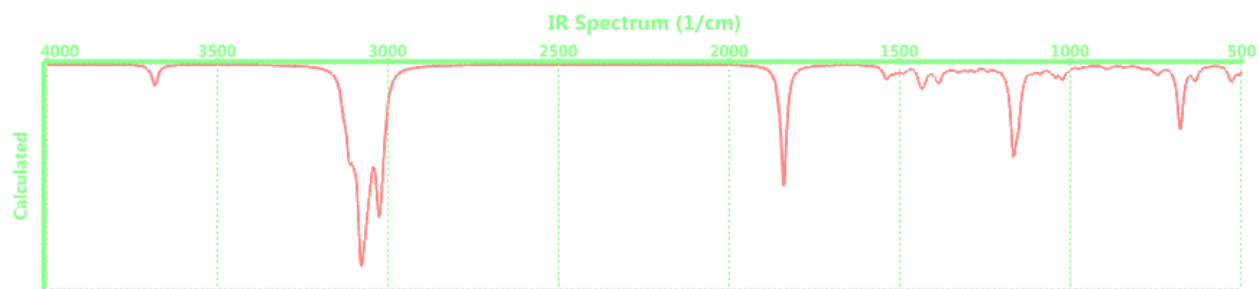


Figure 7 (e): Infra-red spectra of oleic acid using DFT at the B3LYP/6-31G* basis set level